HHS Public Access

Author manuscript

Dev Cell. Author manuscript; available in PMC 2022 July 12.

Published in final edited form as:

Dev Cell. 2021 July 12; 56(13): 1930–1944.e5. doi:10.1016/j.devcel.2021.05.003.

Differential compartmentalization of BMP4/NOGGIN requires NOGGIN trans-epithelial transport

Tien Phan-Everson[#1,2], **Fred Etoc**[#1], **Shu Li**[1], **Samuel Khodursky**[2], **Anna Yoney**[1,2,3], **Ali H. Brivanlou**[1,*], **Eric D. Siggia**[2,4,*]

[1]Laboratory of Stem Cell Biology and Molecular Embryology, The Rockefeller University, New York, New York 10065, USA

[2]Center for Studies in Physics and Biology, The Rockefeller University, New York, New York 10065, USA

[3]Department of Genetics and Development, Columbia University, New York, NY 10032

[4]Lead contact

[#] These authors contributed equally to this work.

SUMMARY

Using self-organizing human models of gastrulation, we previously showed that (i) BMP4 initiates the cascade of events leading to gastrulation; (ii) BMP4 signal-reception is restricted to the basolateral domain; and (iii) in a human-specific manner, BMP4 directly induces the expression of NOGGIN. Here, we report the surprising discovery that in human epiblasts, NOGGIN and BMP4 were secreted into opposite extracellular spaces. Interestingly, apically-presented NOGGIN could inhibit basally-delivered BMP4. Apically-imposed microfluidic flow demonstrated that NOGGIN traveled in the apical extracellular space. Our co-localization analysis detailed the endocytotic route that trafficked NOGGIN from the apical space to the basolateral intercellular space where BMP4 receptors were located. This apical-to-basal transcytosis was indispensable for NOGGIN inhibition. Taken together, the segregation of activator/inhibitor into distinct extracellular spaces challenges classical views of morphogen movement. We propose that the transport of morphogen inhibitors regulates the spatial availability of morphogens during embryogenesis.

[*]Joint Corresponding Authors: brvnlou@rockefeller.edu; siggiae@mail.rockefeller.edu.

AUTHOR CONTRIBUTIONS

Conceptualization: T.P.E, F.E. Investigation: T.P.E, F.E. NOGGIN secretion Western blot: S.L. BMPR immunostaining: S.K. BMP4-KO hESC generation: A.Y. Software: T.P.E, E.D.S. Writing-original draft: T.P.E, F.E, A.H.B., E.D.S. Writing-review and editing: T.P.E, F.E., A.H.B., E.D.S. Supervision: A.H.B., E.D.S.; Funding acquisition: A.H.B., E.D.S. All authors reviewed the manuscript.

DECLARATION OF INTERESTS

F.E. is the Chief Scientific Officer of Rumi Scientific.

E.D.S. and A.H.B. are founders and members of the scientific advisory board of Rumi Scientific.

INCLUSION AND DIVERSITY

We worked to ensure diversity in experimental samples through the selection of the cell lines. One or more of the authors of this paper self-identifies as an underrepresented ethnic minority in science. One or more of the authors of this paper received support from a program designed to increase minority representation in science.

Graphical Abstract

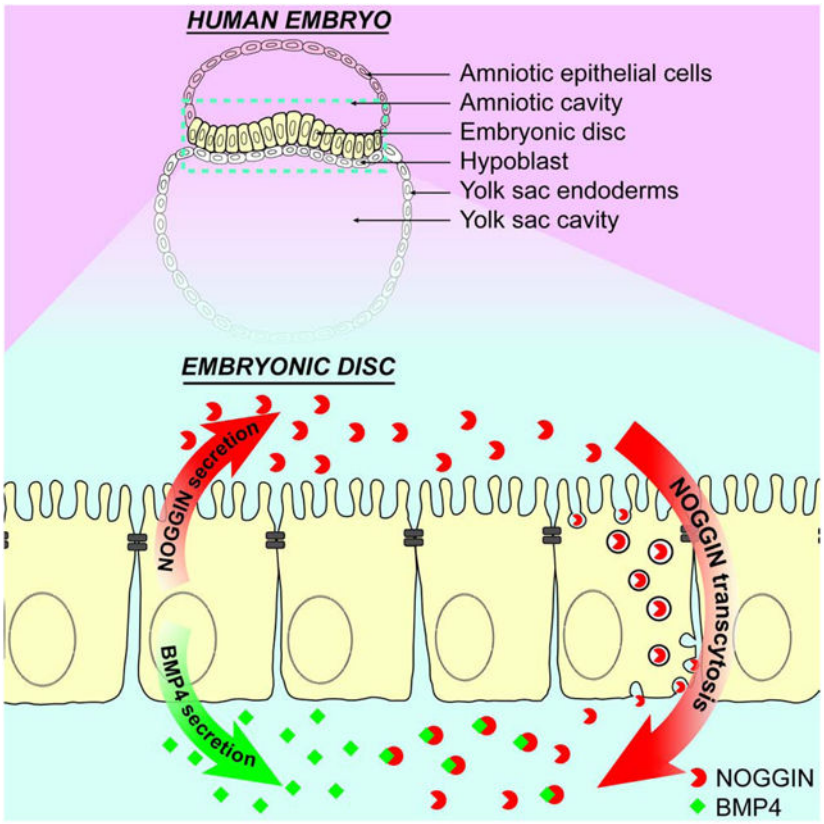

eTOC Blurb

Phan-Everson et al. demonstrates that in a model human epiblast, the morphogen BMP4 and its inhibitor NOGGIN are secreted to opposite extracellular spaces. NOGGIN is then trafficked across the polarized hESC epithelium. Tissue polarity can influence morphogen signaling by restricting the spaces morphogens are secreted to and mediating their transport.

Keywords

human; embryonic stem cells; epiblast; polarity; morphogen; BMP4; NOGGIN; SMAD signaling; transcytosis; endocytosis

INTRODUCTION

Understanding the mechanisms that give rise to spatial patterns in development is a challenge that has intrigued scientists for over a century (Morgan, 1901, Stumpf, 1966, Crick, 1970). One classical mechanism involves morphogens: long-range signaling molecules that control cell fate specification in a concentration-dependent manner. As such, morphogen gradients act as positional cues that direct the patterning of developing tissues during embryogenesis (Warmflash et al., 2012, Rogers and Schier, 2011). It is therefore

critical for morphogenetic cues to be correctly modulated, positioned, and interpreted by the target tissues.

It is often implicitly assumed that morphogens and their secreted inhibitors can freely spread from a source to their point of action. Morphogen spreading is frequently conceptualized and modeled as simple diffusion with decay, though the actual molecular mechanisms are likely to be much more complicated and highly dynamic (Sorre et al., 2014, Kornberg, 2017, Muller et al., 2013, Hidalgo, 2019). Moreover, how morphogen signaling integrates within cellular compartments is mostly unknown; the extracellular micro-environment that contains these diffusive molecules is less well-understood (Yan and Lin, 2009). While model organisms have been instrumental in the dissection of long-range morphogen signaling in early development, the early human embryos have a geometry different from most other model organisms. (Muller et al., 2013, Rogers and Schier, 2011, Wartlick et al., 2009, Wartlick et al., 2014, Zhang et al., 2019). The epithelialized epiblast morphology inherent to the human bilaminar embryonic disc is distinct from the tissue shape of a stage-matched mouse embryo (O'Rahilly and Muller, 2010, Shahbazi and Zernicka-Goetz, 2018, Shahbazi, 2020). Epithelial tissues, which play key roles in shaping human's basic embryonic body plan, consist of a laterally cohesive sheet of cells whose epithelial integrity is maintained by adherens and tight junctions, hence presenting a diffusion barrier (Gilmour et al., 2017). Another defining characteristic of epithelia is a distinct apicobasal polarity which enables apical and basolateral domains to adopt distinct features. As such, signaling is coupled to global embryo as well as local tissue geometry. Although a number of morphogens responsible for embryonic patterning have been identified, we are very far from a quantitative understanding of the dynamics of signaling by these morphogens, which are collectively responsible for transforming a zygote into an embryo.

BMP4 is among the early embryonic morphogens that play critical roles in the patterning of the epiblast (Arnold and Robertson, 2009). We have previously shown that BMP4 alone is sufficient to initiate germ layer self-organization in a gastrulation-like process either in flat 2D micropatterned epiblast model (Etoc et al., 2016), or in a 3D model for primitive streak formation and anterior-posterior symmetry-breaking (Simunovic et al., 2019). Strikingly, our *in vitro* models have revealed that BMP4 reception in the polarized epithelium is restricted to the basolateral cell domain, due to BMP receptors' basolateral localization below the junctional diffusion barrier (Etoc et al., 2016, Zhang et al., 2019, Nallet-Staub et al., 2015). A similar pattern of basolateral receptor localization has also been observed *in vivo* in the developing mouse embryo (Zhang et al., 2019). LTA amino acid motif suggests that this basolateral localization of TGF-β family receptors may be evolutionarily conserved (Zhang et al., 2019).

In contrast to the detailed characterization of morphogens' signaling pathways, the movement of the morphogens' inhibitors has received less attention. NOGGIN – a BMP4 inhibitor – is the first molecule reported to have the properties of a Spemann organizer, inducing dorsal structures (Smith and Harland, 1992). It is well-established that NOGGIN antagonizes BMP4 by binding tightly to BMP4, preventing binding to BMP receptors (Zimmerman et al., 1996). As a human-specific trait, BMP4 induces the direct expression of its own inhibitor NOGGIN, which is required for germ-layer patterning in human models of

gastrulation (Etoc et al., 2016). The mechanisms for NOGGIN spreading and its associated kinetics in embryonic tissue have not been investigated.

In this article, we interrogate the interplay of the morphogen/inhibitor pair BMP4/NOGGIN within our model of the polarized human embryonic disc. Unexpectedly, we found that BMP4 and NOGGIN were selectively secreted into opposite sides of the polarized epithelium, effectively segregating the ligand and its inhibitor into distinct extracellular spaces. Moreover, utilizing a microfluidic flow chamber, we unambiguously demonstrated the long-distance diffusion of NOGGIN through the extracellular medium at the apical side as well as the short-distance diffusion of BMP4 over few direct neighbors. This discovery challenges current dogma which assumes that the morphogen activator and inhibitor diffuse in the same compartment. Surprisingly, we further demonstrate that apically-applied NOGGIN can inhibit basally-applied BMP4 across a tight hESC epithelium, which points to mechanisms of trans-epithelial transport. And finally, we trace the transcytosis route of apical NOGGIN through the endosomal system. Overall, we highlight a complex mechanism where apically-secreted NOGGIN diffuses over long distance in the apical compartment; NOGGIN is then internalized, transcytosed, and trafficked to the basal-lateral surface close to the subcellular locus where BMP receptors are located. Our study shed light on an important and unexpected level of regulation for the transport of morphogen inhibitors whose role in spatially restricting the spread of morphogen signaling ultimately shapes the embryonic body plan.

RESULTS

BMP4 is Secreted Basally and Spreads Locally

Under culture conditions designed for pluripotency maintenance, confluent hESCs form a pseudostratified, apico-basal polarized epithelium reminiscent of the organization of the embryonic epiblast with tight junctions separating the apical and the baso-lateral cell membranes (Supp Fig 1A). As previously shown, hESCs localize their BMP receptors to the basolateral domain just below the tight junctions, making them non-responsive to apically applied BMP4 (Fig 1A) (Etoc et al., 2016). In order to study the signaling dynamics of BMP4 within our model epiblast, we used our own hESC line, RUES2 (NIH# 00012), to stably express transgenes for doxycycline (DOX)-dependent induction of epitope-tagged BMP4 (Fig 1B, Supp Fig 1B–C). We confirmed that these BMP4-secreting cells could induce the expected patterning of various germ layers in a foci-specific manner (Supp Fig 2A–B). BMP4-secreting cells were then transfected with a constitutively expressed nuclear marker, H2B-mCitrine, to allow tracing (Fig 1B). Since secretion can potentially take place from both sides of the polarized epithelium, we cultured the cells on transwell filters, allowing easy access to both apical and basal compartments. At a starting seeding density of ~4,000 cells/mm^2; the cells form a confluent, polarized epithelium on the filters after 22 hrs in culture (Supp Fig 1A). This defines our set of standard conditions for the culture of our model epiblasts.

We used DOX to induce RUES2 on transwell filters to produce BMP4 then probed for secreted BMP4 in the apical and basal compartments. BMP4 was found nearly exclusively in the basal media for up to 24 hrs (Fig 1C). We then characterized BMP4 lateral spreading

dynamics by mixing a low proportion (1:200) of BMP4-producing hESCs within a WT hESCs background. This allowed us to quantify the spatial range of BMP4 propagation in the WT "receiving" cells by quantifying nuclear phosphorylated SMAD1/5/8. Starting at 8 hrs post-induction, basally-secreted BMP4 activated nuclear pSMAD1/5/8, first in an autocrine manner in the secreting cells. At later time-points, a paracrine signal – which could be fitted by an exponential decay function – spread through the epithelium and reached a characteristic length of 20 μm from the closest secreting cells after 24 hrs (Fig 1D–E).

To further characterize the contribution of WT "receiving" cells to BMP4-dependent pSMAD1/5/8 propagation, we generated a stable line of BMP4-KO hESCs (Supp Fig 1D–E). We mixed a low proportion (1:200) of BMP4-producing hESCs within a background of BMP4-KO or WT hESCs. We observed that the spatial range of pSMAD1/5/8 propagation was similar in WT and BMP4-KO hESCs (Supp Fig 2C–D). Our result suggests that the observed pSMAD1/5/8 signal propagation was driven by BMP4 ligands overexpressed by the BMP4-producing hESCs and not by endogenous BMP4 secreted by "receiving" cells.

NOGGIN is Secreted Apically and Forms a Concentration Gradient

Since NOGGIN is expressed as a response to BMP4 (Etoc et al., 2016), we then asked whether NOGGIN propagated with the same characteristics as BMP4, i.e. basal secretion with short-ranged lateral propagation. Similar to the strategy we employed for studying BMP4 propagation, we generated an RUES2 line stably incorporating a transgene for doxycycline-dependent induction of epitope-tagged NOGGIN together with a constitutively expressed H2B-mCherry nuclear marker (Fig 2A). The level of NOGGIN produced by these inducible NOGGIN-secreting cells was higher than that produced as a response to BMP4 stimulation (Etoc et al., 2016) (Supp Fig 3A). Compared to BMP4, in our induction assay on transwells, secreted NOGGIN could be detected at earlier time points. To our surprise, we found that V5-tagged NOGGIN was exclusively secreted to the apical media after 2-, 4-, and 8-hr induction (Fig 2B). As such, the ligand BMP4 and its inhibitor NOGGIN were secreted into opposite extracellular spaces.

We next examined the dynamics of NOGGIN transport within our model epiblast by seeding a low dilution of NOGGIN-producing cells in a background of WT-RUES2. We applied DOX for different durations to induce secretion of NOGGIN, followed by a brief 1 hr pulse of BMP4 presented to the basal media. Spatial domains of BMP4 activity were highlighted by pSMAD1/5/8 staining. As expected, NOGGIN-producing cells effectively prevented BMP4-dependent initiation of pSMAD1/5/8 autonomously and non-autonomously. The spatiotemporal range of NOGGIN inhibition was defined by the area of pSMAD1/5/8-negative hESCs surrounding the NOGGIN-producing cells (Fig 2C). The range of inhibition extended from 13 μm (at 4 hrs) to 150 μm (at 24 hrs) (Fig 2D).

Finally, we probed the concentration profile of NOGGIN away from a secreting source. To this end, we induced diluted NOGGIN-producing cells for a defined period of time (6 hrs) and then challenged the tissue globally via basal application of different concentrations of BMP4. As expected, NOGGIN's efficiency in counteracting pSMAD1/5/8 induced by basally-applied BMP4 was inversely proportional to BMP4 concentration: the inhibition

rings around the NOGGIN-producing cells had decreasing radii as BMP4 concentration increased (Fig 2E–F). This result demonstrates that the activity of NOGGIN away from a source was indeed graded.

Apically-Applied NOGGIN Can Inhibit Basally-Applied BMP4

That BMP4 and NOGGIN are secreted into different extracellular spaces is surprising since NOGGIN has to directly bind BMP4 in order to prevent its interaction with BMP receptors and block signaling. Where and how can two proteins, in different compartments separated by a diffusion barrier - the tight junctions, meet and interact? In order to address this question, we first set up a series of time-course Western blot analysis of cell lysates probing for for pSMAD1/5/8 activation under different signaling conditions. Specifically, we recorded the level of pSMAD1/5/8 following a pulse or a sustained application of BMP4. The efficacy of apically-applied NOGGIN in inhibiting pSMAD1/5/8 was then compared to that of known BMP4 inhibitor LDN. As expected, a sustained basal application of BMP4 resulted in sustained pSMAD1/5/8 response, while a single short pulse of BMP4 generated a response that lasted 3 hrs (Fig 3A). Most strikingly, addition of NOGGIN in the apical compartment completely shut down ongoing BMP4 signaling within 2 hrs. Thus, NOGGIN trafficking from apical to basal occurs within a 2-hr window. pSMAD1/5/8 inhibition by apical NOGGIN occurred slower compared to inhibition by the small compound inhibitor LDN, and yet faster than when BMP4 was removed after a pulse (Fig 3A). Moreover, NOGGIN's inhibitory effect was maintained for up to 3 hrs after NOGGIN washout (Supp Fig 3B). This result is consistent with previous report that NOGGIN binds strongly to heparan sulfate proteoglycans on the cell surface (Paine-Saunders et al., 2002).

To independently control for physiological morphogen levels and kinetics, we tested the efficacy of NOGGIN inhibition in a context of BMP4 expressing cells. BMP4-producing cells, diluted in a background of WT-RUES2, were induced to secret the ligand. The epithelium was then challenged with various concentrations of recombinant NOGGIN, applied apically or basally. While basally-applied NOGGIN was most effective at inhibiting BMP4 signaling, apically-applied NOGGIN was also capable of switching off sustained BMP4 signaling in a dose-dependent manner (Fig 3B–C). Analysis by Western blot confirms that apical NOGGIN rapidly quenches the response to a preceding pulse of BMP4 (Supp Fig 3C).

Overall, these experiments demonstrate that apically-applied NOGGIN functionally and efficiently inhibits basal BMP4, and with similar kinetics as basal BMP4 washout. Moreover, retention of the inhibitory effect after NOGGIN washout suggests mechanisms of internalization and trafficking of NOGGIN from the apical to basal compartment where BMP4 is present.

NOGGIN Diffuses Across the Apical Compartment

We hypothesized that diffusion in the extracellular medium at the apical side was a major mechanism for NOGGIN's long-range propagation in the epithelium. To test this, we customized a glass-bottomed microfluidic culture platform, which supported controlled perfusion flow rates, and applied apical laminar flow (Material and Methods, Supp Fig

4A–C). This microfluidic system supported the epithelialization of hESCs while maintaining their pluripotency at both low and high flow rates (Supp Fig 5A–B). We also confirmed that both glass and filter substrates led to similar BMP4 signaling range and spreading dynamics (Supp Fig 5C–D, Fig 1D).

We utilized this microfluidic device to validate our hypothesis by demonstrating that by briefly switching a flow of 10 μl/hr to a high flow rate of 1000 μl/hr, we can wash away secreted NOGGIN at the apical side and lessen or eliminate its inhibition. Since we have demonstrated earlier that BMP4 was basally secreted, application of an apical flow should not perturb its local spreading. As a control, we diluted BMP4 secreting cells into the WT-RUES2 epithelium at a ratio of 1:200, which allowed us to quantify the spread of pSMAD1/5/8 activity around isolated BMP4 sources (Fig 4A–B). After 6 hrs of doxycycline induction, no difference in BMP4 signaling ranges between low and high flow regimes was detected, except for an increase in the amplitude of pSMAD1/5/8 intensity, in the high flow condition, consistent with a washout of endogenous inhibitors induced by BMP4 stimulation (Etoc et al., 2016). This minimal effect of flow on BMP4 lateral spreading is consistent with BMP4's basal secretion and its uptake in nearby cells.

Increasing the ratio of BMP4-secreting cells in WT-RUES2 to 1:10 led to uniform expression of pSMAD1/5/8 in both low and high flow conditions (Fig 4C). However, when a small number of NOGGIN-secreting cells (1:500) were added, this pSMAD1/5/8 expression was inhibited at low flow rate (Fig 4D). In contrast, high apical flow showed active BMP4 signaling only in cells a distance away from NOGGIN-secreting cells (Fig 4D, Supp Fig 4D). Thus, high apical flow reduced NOGGIN inhibition spread consistent with its apical secretion and activity when apically supplied. The persistence of BMP4 inhibition specifically around the NOGGIN-secreting cells in the high flow condition argues that the flow was neither generically activating BMP4 signaling by another route such as shear stress, nor washing out some unknown inhibitor. Moreover, the shear rate on the cells at the highest flow is 0.03 dynes/cm^2 which is 30 times less than the lowest value that elicits a response in endothelial cells (Ballermann et al., 1998). The simplest explanation of our data is thus that the flow washed away NOGGIN and precluded its transport to the cells furthest from the NOGGIN secreting cells. Overall, these experiments concur that NOGGIN traveled in the apical extracellular space while BMP4 used the basolateral space.

NOGGIN's Subcellular Localization

To further examine how apically-spreading NOGGIN protein trafficked intracellularly to inhibit BMP4, we mixed a small number of NOGGIN-secreting with WT-RUES2 (1:100) and assessed the subcellular localization of NOGGIN throughout the layer by staining the V5 tag after 8 hrs of induction followed by 1 hr of basal BMP4 application (Fig 5A). As expected for secreting cells, high concentration of NOGGIN was found in the golgi (Supp Fig 5E). pSMAD1/5/8 expression delineated the range of NOGGIN activity in surround cells (Fig 5A–B). Unexpectedly, however, in receiving cells, NOGGIN was mostly found at the basolateral domain. Quantification of NOGGIN localization in the Z plane indicated that NOGGIN consistently localized below tight junctions as demarcated by ZO-1 labeling (Fig 5C). This NOGGIN lateral accumulation tightly overlapped with the expression patterns

of BMPR1a and BMPR2 (Fig 5D–E). In addition to labeling the baso-lateral domain, NOGGIN immunostaining also appeared as discrete puncta of various sizes, dispersed in the cytoplasm, indicative of endocytic vesicles in the apical pole of the cells, both at and below the level of tight junction marker ZO-1 (Fig 5F). Taken together, our results suggest that following apical secretion from the source, NOGGIN enters receiving cells on the apical side, trafficks through endocytotic vesicular compartments, and ultimately reaches the basolateral side near BMP receptors.

NOGGIN Trans-Epithelial Transport

We suspected that trafficking of NOGGIN was a prerequisite for its effect on pSMAD1/5/8 levels. Taking advantage of the physical properties of the plasma membrane, lowering the temperature of the cell culture is a commonly used method for nonspecific inhibition of endocytosis (Brunner et al., 2020). WT-RUES2 were first basally stimulated with BMP4, then NOGGIN was added apically or basally either at 37°C or at 4°C. At 4°C, the inhibitory effect NOGGIN has on pSMAD1/5/8 was eliminated, regardless of whether NOGGIN was added apically or basally (Fig 6A–B). This result suggests that the trafficking of NOGGIN is crucial for its modulatory effect on BMP4 signaling.

We then hypothesized that NOGGIN was endocytosed specifically via clathrin-dependent endocytosis, similar to BMP2 and BMPR (Hartung et al., 2006, Paarmann et al., 2016). In order to probe NOGGIN endocytosis, we took advantage of the small molecule Dyngo4a which inhibits dynamin – an essential regulator for the internalization of endocytotic vesicles via clathrin-mediated endocytosis and micropinocytosis (McCluskey et al., 2013). When recombinant NOGGIN was presented to the apical or basal compartment, the protein was internalized as demonstrated by Western Blot on the cell lysates. Only apical internalization was effectively blocked by Dyngo4a concurrent treatment, demonstrating the specific requirement for dynamin in apical NOGGIN uptake (Fig 6C–D). On the other hand, Dyngo4a pre-treatment did not affect BMP4 signaling (Supp Fig 6A).

Various other pharmacological inhibitors of endocytosis were tested for their efficacy in inhibiting NOGGIN internalization (Table 1). Of all inhibitors tested, Dyngo4a remained the most efficient at suppressing NOGGIN apical internalization (Supp Fig 6B–C). Our result suggests that NOGGIN apical internalization was actin-dependent and could be mediated via different endocytotic mechanisms such as clathrin-dependent endocytosis, caveolae-dependent endocytosis, and micropinocytosis. It is worth noting that although pharmacological inhibitors are convenient to use, their specificity and cell-type-dependency remain an issue (Ivanov, 2008, Vercauteren et al., 2010, Dutta and Donaldson, 2012).

We next tested whether NOGGIN underwent apical-to-basal transcytosis. To this end, we collected V5-tagged-NOGGIN-conditioned media from the apical culture media of NOGGIN-secreting cells. This conditioned media was applied to the apical compartment atop polarized hESC epithelium for up to 48 hrs. Consistent with transcytosis, V5-tagged-NOGGIN was recovered in the opposite side of the filter, in the basal compartment starting at 36 hrs after application (Fig 6E). Following the experiment, immunofluorescence and permeability assays were performed on the same hESC samples to confirm epithelial barrier integrity (Supp Fig 6D–F). This demonstration of NOGGIN transcytosis explains

the detection of NOGGIN in the basal media at 24 hrs in the NOGGIN secretion experiment (Fig 2B). The difference in timeline for NOGGIN basal detection in these two experiments can be explained by the difference between continuous NOGGIN production in the secretion experiment and gradual NOGGIN degradation within the conditioned media in the transcytosis experiment. Together, these results again support the hypothesis that NOGGIN undergoes apical-to-basal transcytosis.

Next, to dissect the specific endocytotic pathways associated with NOGGIN transport, we carried out a series of co-localization analyses between NOGGIN and various endosomal markers. The presence of NOGGIN in specific endosomal compartments: pinocytotic vesicles, apical sorting endosomes (ASE), early endosomes (EE), apical recycling endosomes (ARE), common recycling endosomes (CRE), and basal sorting endosomes (BSE) was measured by quantitative immunofluorescence co-localization (Sheff et al., 1999, Perez Bay et al., 2016, Lapierre et al., 2012, Li et al., 2015, Cresawn et al., 2007, Simonsen et al., 1998, Brown et al., 2000, Knight et al., 1995, Odorizzi et al., 1996). NOGGIN-producing cells diluted in a WT hESC epithelium (1:100) were induced to secrete NOGGIN for 24 hrs. Paired immunostaining of V5 and multiple endosomal markers was then performed in receiving cells, followed by co-localization analysis. Confocal microscopy was able to resolve domain-selective labeling of the markers for pinocytotic vesicles, ASE, and ARE: pinocytotic vesicles and ASE were found exclusively in the apical region while the majority of ARE was found in the supranuclear region (Fig 6F). The distribution of the total overlap between NOGGIN and each endosomal marker in all z-positions was computed (Fig 6 G–H). NOGGIN's z-profiles (Supp Fig 7A) and each corresponding endosomes' z-profiles were plotted in the z-plane relative to the tight junction marker ZO-1 (Supp Fig 7B) (for summary of endosomal markers, see Fig 7; for full protocol description, see Methods). Co-localization profiles (Supp Fig 7C) indicate that most of the co-localization between NOGGIN-V5 and endosomal markers occurred at the level at or below tight junctions.

The fraction of NOGGIN-V5 that co-localized with each endosomal marker at different z-positions was computed. The overlap data (left axis, black) was graphed against the fluorescence profile of the respective endosome (right axis, green) (Fig 6I). V5 labeling was found to localize with markers for pinocytotic vesicles (labeled by Dextran-10'), ASE (labeled by WGA-10'), EE (labeled by early endosome antigen 1 EEA1), CRE (labeled by Transferrin-45'), and BSE (labeled by Transferrin-5'). Co-localization was not observed between V5 and ARE (labeled by Rab11a). To verify that the co-localization fraction represented valid, meaningful localization, the fraction of endosomal markers that co-localized with NOGGIN was graphed against the fluorescence profile of the respective endosome (Supp Fig 7D). Thus these results suggest that upon endocytosis by pinocytotic vesicles, NOGGIN travels through EE and ASE before arriving at the CRE. From the CRE, NOGGIN is directed to the BSE and finally targeted for exocytosis to the inter-cellular space where BMP receptors are localized at the basolateral membrane (Fig 7).

DISCUSSION

The surprising observation that in a model human epiblast, a pair of secreted morphogen and inhibitor that directly bind each other are in fact initially secreted into opposite extracellular spaces forces a reconsideration of our current understanding of the molecular mechanisms underlying embryonic pattern formation. That BMP4 is secreted baso-laterally is consistent with the localization of the BMP receptors (Etoc et al., 2016, Zhang et al., 2019). NOGGIN apical secretion into an opposite compartment separate from BMP4, which was not anticipated by current models, might represent a necessary mechanism as it would prevent immediate binding and inactivation of both factors and thus enable their patterning roles over large distances.

The spread of BMP4 and NOGGIN activity from a localized source was consistent with Turing's reaction-diffusion model, which postulates that the inhibitor must travel faster than ligand. The spread of NOGGIN was long-ranged, and almost 8 times greater than the lateral spread of BMP4 which remained restricted to only 2–3 adjacent cell neighbors. The differential diffusion rates may be regulated by the extracellular matrix as NOGGIN and BMP4 bind components of the extracellular matrix with different affinities (Rider and Mulloy, 2017, Paine-Saunders et al., 2002, Ohkawara et al., 2002). Additionally, the biophysical and geometrical properties of the apical and basal extracellular compartments differ. Therefore, the possibility that secreted molecules generally diffuse further at the apical side than at the basal side cannot be excluded. This situation has been shown to be the case in the luminal cavity of the implanting mammalian embryo, where the amniotic cavity on the apical side of the epithelia allows for the rapid transport of secreted factors, potentially to concentrate and homogenize inhibition through all cells lining the lumen (Simunovic et al., 2019, Zhang et al., 2019).

The polarized secretion of NOGGIN and BMP4 exemplifies how an epithelium can create a sharp boundary within an embryo. Cells on the apical side would have BMP inhibited while those on the basal side would experience BMP signaling. This phenomena was recently proposed in connection with WNT signaling in the developing epidermis where a single-layer multipotent epithelial progenitor defines the boundary between WNT activity on its basal side and WNT repression on its apical side (Matos et al., 2020). Moreover, it becomes increasingly clear that during gastrulation, while important signals are supplied by the visceral endoderm or hypoblast, signal reception is controlled by epithelial cell polarity (Zhang et al., 2019, Etoc et al., 2016). How epithelial cell types integrate morphogen signals will have to be incorporated in models of epiblast symmetry breaking to understand communication between embryonic and extra-embryonic populations.

Epithelial polarity also operates to control vesicular trafficking machineries and regulates vectorial transport (Rodriguez-Boulan et al., 2005, Rodriguez-Boulan and Macara, 2014). We have traced the path of NOGGIN from the early sorting endosomes on the apical side, to the basal sorting endosomes, and finally to the baso-lateral location next to the BMP receptors. The baso-lateral targeting of NOGGIN makes sense as it might be more efficient for an inhibitor to shield a small pool of very localized receptors than a diluted batch of ligand distributed through the more extended extra-cellular space. However, while we have

shown that NOGGIN can undergo transcytosis and neutralize basally-introduced BMP4, the location where NOGGIN first interacts with BMP4 remains ambiguous. It remains unclear whether NOGGIN directly enters the same pool within endosomal compartments as BMP4, or whether BMP4 is constitutively degraded after endocytosis (Hartung et al., 2006; Paarmann et al., 2016). Our study therefore does not eliminate the possibility that BMP4 and NOGGIN meet inside transport vesicles.

Limitations of the Study:

One caveat of our experimental design is that in the absence of detection methods to visualize endogenous signals, we had to rely on over-expression systems which produce protein levels higher than those found *in vivo*. However, time- and concentration-response curves show smooth variations, and our results for exogenously applied BMP4 or NOGGIN are consistent with those from the DOX induced cell lines. Thus, cells at a distance from the source do experience a graded concentration profile. These cells at the boundary near those that do and do not respond to pSMAD1/5/8 encounter relevant concentrations of morphogen/inhibitor. Therefore, given the limitation of current technologies, we believe the cellular responses occurring at the boundary are indicative of what happens *in vivo*. Another notable point of discussion is that although the endocytotic vesicles described in this study transport the bulk of NOGGIN transcytosis, not 100% of NOGGIN is accounted for. Therefore, there may be other unidentified endocytotic vesicles involved in NOGGIN's apical-to-basal transcytosis.

We showed previously that ACTIVIN/NODAL receptors are also baso-laterally localized in human gastruloids grown in confined geometry as well as when cultured on filters (Etoc et al., 2016). It is therefore tempting to speculate that a similar scenario between ligands and inhibitors might be at play. Indeed, ACTIVIN/NODAL inhibitors such as LEFTY1/2 and CERBERUS have also been shown to be induced directly by activation of the SMAD2/3 pathway (Yoney et al., 2018). Interestingly, we did not observe an apical-basal asymmetry in the reception of recombinant WNT3A protein in our RUES2 colonies (Martyn et al., 2019). While this suggests that these types of segregated secretion of ligands/inhibitors might be unique to the TGFβ signaling pathway, we note that in the Drosophila wing, transcytosis of Wnt from the apical to basal compartment and its inhibition by Notum are essential for patterning (Yamazaki et al., 2016). Thus, as in the case of human-specific induction of NOGGIN by BMP4, these might represent species-specific attributes. Probing signaling dynamics in other polarized epithelia holds the promise of unveiling more surprises.

Stem cell-based, self-organizing models of human development provide a robust tool to discover early aspect of human embryogenesis which otherwise would be impossible to scrutinize (Tyser, 2020). Among many other contributions, these tools allowed for the discovery of polarized signal reception in hESC colonies and its *in vivo* relevance for BMP4 signaling in the amniotic cavity of the mouse embryo (Etoc et al., 2016, Zhang et al., 2019). This scenario can be reiterated overtime during multiple stages of embryonic development. For example, the early neural tube consists of a polarized epithelium that both sends and receives multiple signals. In mouse, NOGGIN and SHH secreted from the floor plate and notochord impinge on the cells of the ventral neural tube, while BMP4

secreted from the roof plate and ectoderm impinges on the cells of the dorsal neural tube (Brent and Tabin, 2002, McMahon et al., 1998, Ybot-Gonzalez et al., 2007). Thus, polarized secretion and reception may play a role in dorsal/central specifications and subsequently influence surrounding tissues such as neural crests and somites. Therefore, epithelial polarity represents part of the toolkit used by embryos for robust developmental patterning through secreted molecules.

STAR*METHODS

RESOURCE AVAILABILITY

Contact for Reagent and Resource Sharing—Further information and requests for resources and reagents should be directed to and will be fulfilled by the Lead Contact, Eric Siggia (siggiae@mail.rockefeller.edu)

Material availability—All unique reagents generated in this study are available from the Lead Contact without restriction.

Data and code availability—This study did not generate any unique datasets.

The Matlab code used to quantify pSMAD1/5/8 signal propagation can be found at: https://github.com/tphan219/pSMAD_SignalPropagation

EXPERIMENTAL MODEL AND SUBJECT DETAILS

Routine hESC line maintenance—Experiments were performed with RUES2 hESC line (NIH hESC-09–0013; RRID:CVCL_B810). Cells were tested for mycoplasma infection before beginning experiments and then again at 2-month intervals. Cell lines were routinely maintained on tissue culture dishes coated with Matrigel (BD Biosciences, 1:40 dilution). Dishes were coated in Matrigel overnight at 4 °C and then incubated at 37 °C for 1 h immediately before the cells were seeded on the surface. All hESC lines were grown in HUESM medium (DMEM supplemented with 20% knockout serum replacement, 1×B27 supplement without vitamin A, 0.1 mM non-essential amino acids, 2 mM GlutaMax and 0.1 mM 2-mercaptoethanol) that was conditioned by mouse embryonic fibroblasts (MEF-CM) and supplemented with 20 ng/ml bFGF. The medium was changed daily. Cells were passaged as aggregates using ReLeSR (Stem Cell Technologies), or as single cells using Accutase (Stem Cell Technologies).

Cell line generation—Human Noggin cDNA was amplified by PCR from a cDNA clone obtained from Thermo Scientific (MHS6278–202841236). V5 tag was inserted at the N-terminal end for NOGGIN, upstream of the start codon by insertion into the PCR primers. Construct for the expression of Myc-tagged xBMP4 was generated previously (Degnin et al., 2004, Cui et al., 2001). The inserts were then separately cloned into a bi-cistronic vector expressing constitutively a puromycine resistance. The gene to be expressed was placed downstream of the Tet responsive element (Fig. 1B and Fig 2A). The CRISPR/Cas9 system was used to generate a BMP4-Knockout RUES2 hESC line by targeting exon 3 of the BMP4 gene (ENGS 125378) (Supp. Fig. 1B).

Nucleofection was carried out using the Cell Line Nucelofector Kit L (Lonza, Walkersville, MD) and the B-016 setting of a Nucleofector II instrument. Nucleofected cells were plated into MEF-CM supplemented with 10 μM Rock-inhibitor. Antibiotic selection was started at day 4 and continued for 7 days. Cells that survived selection were passaged as single cells using Accutase, plated in MEF-CM supplemented with 10 μM Rock-inhibitor, and allowed to grow into colonies. Colonies arising from a single cell were handpicked, expanded, and screened for correct targeting by PCR amplification of the genomic region and Sanger sequencing. Correctly targeted clones were subsequently transfected with ePiggyBac plasmids containing a nuclear marker (H2B-mCitrine or H2B-mCherry cassettes) (Lacoste et al., 2009). Individual clones were again isolated and controlled for normal karyotype (G-banding) and pluripotency maintenance. Once the clones had been successfully established, they were assayed functionally: brightness for the morphological reporter, pSMAD1/5 activation for the BMP4-expressing line, BMP4 inhibition for the NOGGIN-expressing line, and BMP4 mRNA expression for the BMP4-KO lines.

All cell lines were sequenced and karyotyped (GTL banding; Cell Line Genetics) as part of routine culture quality control.

2D model epiblast—Except the microfluidic experiment, all experiments were done with hESCs grown on transwell filters. Transwell polycarbonate membrane (Corning, 3413) inserts, 6.5 mm in diameter, were coated for 2 h at 37 °C with 100 μl of 10 mg ml^{-1} laminin 521 (BioLamina) diluted in PBS+ / +. The membrane was rinsed with PBS+ / +. The cells were dissociated as single cells with Accutase and then resuspended in MEF-CM + 20 ng ml^{-1} bFGF + 10 μM RI. The same medium containing 200,000 cells in 100 μl was added on top of the membrane and 600 μl of the same medium (without cells) was added to the bottom of each filter insert. This volume condition kept the culture system in hydrostatic equilibrium. The RI was washed out 2 h later (from both filter compartments). 18–20 h after seeding, MEF-CM + 20 ng ml^{-1} bFGF + 0.2 μg ml^{-1} doxycyline was added to the top and bottom chambers if induction of expression vectors was required. 0.2 μg ml^{-1} doxycyline was determined to be the saturating dose for the overexpression of TRE::NOGGIN-V5 hESCs (Supp Fig 3A).

If media were to be collected for western blotting, E8 medium (STEMCELL Technology) + 0.2 μg ml^{-1} doxycyline was used instead because serum produced by MEF-CM causes large non-specific bands that confound analysis.

METHOD DETAILS

qPCR—WT RUES2 hESCs were cultured on Transwell filters. 18–20 h after seeding, doxycycline (0, 0.01 μg ml^{-1}, 0.05 μg ml^{-1}, 0.2 μg ml^{-1}, and 1 μg ml^{-1}) or recombinant BMP4 (0 ng ml^{-1}, 10 ng ml^{-1} and 50 ng ml^{-1}) was added to the transwell for 2 h, 6 h, or 12 h. Cells were lyzed in Trizol (Thermo Fisher Scientific) and their total RNA was isolated using RNeasy mini kit (QIAGEN). cDNA was synthesized using the Maxima H Minus First Strand cDNA Synthesis Kit (Life Technologies). qRT-PCR for selected genes were performed using PowerUp SYBR Green Master Mix (Life Technologies) in a QuantStudio 6 Pro PCR Systems (Applied Biosystems).

Immunostaining—At specified time points, filters were fixed with 4% PFA (Electron Microscopy) for 20 min, washed twice with PBS, permeablized with 0.5% Triton X-100 in PBS (PBST) for 15 min, and then blocked with 3% normal donkey serum in 0.1% PBST for 1 h. Cultures were incubated overnight with primary antibodies in this blocking buffer at 4°C, washed three times with 0.1% PBST for 30 min each, and then incubated with secondary antibodies (diluted 1:500) (Life Technologies: donkey anti-rabbit, donkey anti-mouse or donkey anti-goat antibodies conjugated with Alexa Fluor 488, 555 or 647) and DAPI (1 ug ml^{-1}) in blocking solution for 1 h before being washed three times with 0.1% PBST for 30 min each. Transwell filters were removed from the inserts and mounted with excess ProLong Gold antifade mountant (Invitrogen) onto glass coverslips. Coverslips were sealed with nail polish before antifade mountant dries to preserve cellular structures in the z-plane.

Endosome labeling—Culture of cells on filters were prepared as described above. Cells were stimulated with 0.2 μg ml^{-1} doxycycline for 24 hrs prior to endosome labeling.

Endosome labeling protocols for ASE, BSE, and CRE were adapted from (Perez Bay et al., 2016). In short, the ASE is labeled by 5-minute apical incubation with WGA-FITC (Sigma-Aldrich, L4895), the BSE by 5-minute basal incubation with transferrin-CF488, and the CRE by 45-minute basal incubation with transferrin-CF488 (Biotium, #00081). Macro- and micro-pinocytosis vesicles were labeled by 10-minute apical incubation with 10kDA Dextran-FITC (Li et al., 2015). The ARE and EE were labeled via immunofluorescence by Rab11A and EEA1, respectively. Following labeling of endosomal compartments, cells were processed for immunolabeling as described above.

Imaging—All confocal images were acquired on Inverted Zeiss LSM 780 laser scanning confocal microscope (Zeiss) with a 20x/0.8 numerical aperture (NA) or 60X/1.4 NA oil-immersion objective lens. The confocal pinhole was set to 1 Airy unit. For z-stacks, the z-spacing was 0.5 μm.

Western blotting—Cell lysate collection: After being briefly washed with cold PBS+ / +, cells were directly lysed on filters with RIPA lysis and extraction buffer (Thermo Scientific) supplemented with 1X proteinase inhibitor as per manufacturer's recommendation for monolayer-cultured mammalian cells.

Medium collection: Media from the apical and basolateral chambers were collected directly from transwell filters. Due to the differential volumes used in culture, the apical medium was diluted 6x to normalize to the basal medium. Samples were supplemented with 1X proteinase inhibitor (Thermo Scientific) before being centrifuged at ~14,000 × g for 15 minutes to remove cell debris.

For all western blotting experiments, collected samples were denatured and reduced in NuPAGE LDS buffer (Invitrogen) and NuPAGE reducing reagent (Invitrogen) at 70°C for 10 minutes. SDS-PAGE in 4–15% Mini-PROTEAN TGX precast gels (BIO-RAD) under reducing conditions was performed. Protein transfer was performed with Trans-Blot® Turbo™ Mini PVDF (BIO-RAD) according to manufacturer's instructions.

Following transfer, membranes were blocked with 5% non-fat dried milk in 1X Tris-Buffered Saline with 0.1% Tween® 20 Detergent (TBST) for 1 h. Membranes were incubated overnight with primary antibodies in 3% BSA in TBST at 4°C. After 3 15-minute washes with TBST, membranes were incubated with secondary antibodies (AffiniPure Fab Fragment Donkey Anti-Rabbit or Donkey Anti-Mouse IgG; Jackson ImmunoResearch Lab) in 3% BSA in TBST for 1 h. After 3 15-minute washes with TBST, detection was performed with Pierce™ ECL Western Blotting Substrate (Thermo Scientific) or SuperSignal West Femto Maximum Sensitivity Substrate (Thermo Scientific), following manufacturer's instructions.

Transcytosis inhibition—WT RUES2 hESCs were cultured on Transwell filters as described above. 250 ng ml^{-1} recombinant human NOGGIN (R&D Systems; 6057) was added to the apical compartment. For nonspecific inhibition of endocytosis, the filters were moved to 4°C for 2 hours. For pharmacological inhibition of endocytosis, inhibitors were individually added to the apical compartment for 2 hours; the final concentrations of each inhibitor are listed in Supplementary Table 1. After 2 hours, the cell lysates were collected and processed for Western blotting as described previously.

References for the use of pharmacological inhibitors are listed in Supplementary Table 1: (Abassi et al., 2009, Akiyama et al., 1987, Aoki et al., 1999, Delvaux et al., 1990, Dutta et al., 2012, Fujimoto et al., 2000, Hamm-Alvarez et al., 1996, Harasztosi et al., 2018, Hoebeke et al., 1976, Huang et al., 2017, Jackman et al., 1994, Koivusalo et al., 2010, Lagana et al., 2000, Linstedt and Hauri, 1993, Mayer et al., 1999, Nabi and Le, 2003, Park et al., 2013, Sampath and Pollard, 1991, Schliwa, 1982, Subtil and Dautry-Varsat, 1997, Vasquez et al., 1997, von Kleist et al., 2011, Wang et al., 1993, Yao et al., 2017, Witte et al., 2020, Willox et al., 2014)

Microfluidic device fabrication—75 × 25 mm glass slides (VWR) were sonicated in acetone and isopronanol for 20 min each and rinsed with deionized water.

The custom microfluidic device consisted of a polymethylsiloxane (PDMS) structure layer having a flow channel sandwiched between two glass slides. The PDMS structure layer was made by mixing PDMS curing agent and base polymer (Sylgard 184; Dow Corning) at a ratio of 1:10 before casting PDMS prepolymer onto a 3D-printed mold and baking at 40°C for 12 h. On one side, the PDMS layer was permanently attached via plasma bonding to a glass slide which had custom-drilled inlet and outlet holes (1.2-mm diameter). On the other side, the PDMS layer was reversibly attached via surface adhesion to another glass slide which would provide the surface for cells to be cultured. This reversible attachment allowed for easy disassembly of the flow chamber system and removal of the glass slide containing the cell epithelium, thus simplifying subsequent immunostaining steps.

The completed flow cell was inserted into a custom metal clamping frame where inlet and outlet tubing was screwed on for a tight seal (Supplementary Fig. 1). Before usage, the microfluidic device was sterilized under UV light for 30 min.

Microfluidic flow assay—Microfluidic chambers were coated for 2 hrs at 37 °C with 100 µl of 10 mg ml^{-1} laminin 521 (BioLamina) diluted in PBS+ / +. The cells were dissociated as single cells with Accutase and then resuspended in MEF-CM + 20 ng ml^{-1} bFGF + 10 µM RI + 100 U ml^{-1} penicillin–streptomycin. The same medium containing 4×10^6 cells ml^{-1} was slowly flowed in to the chamber at a rate of 100 µl $minute^{-1}$ until the chamber surface was covered evenly and entirely by cells. 2 h later, the RI and excess cells were flowed out at a rate of 3 ml h^{-1}; then, the flow rate was set to 10 µl h^{-1}. 30–36 h after seeding, if induction of expression vectors was required, MEF-CM + 20 ng ml^{-1} bFGF + 0.2 µg ml^{-1} doxycyline was quickly flowed in at a rate of 3 ml h^{-1} for 30 minutes. The flow rate was then set to 10 µl h^{-1} or 1000 µl h^{-1} for minimal flow or high flow conditions, respectively. After 6 hrs, 4% PFA (Electron Microscopy) was quickly flowed into the chamber and the epithelium was fixed for 20 minutes. The microfluidic chamber was then disassembled, and the epithelium on glass slide immunostained as described above.

Transcytosis—Collecting NOGGIN-conditioned medium: RUES2-ePB-TRE::V5-NOGGIN cells were cultured on Geltrex-coated dishes (Thermo Fisher; A1413302) at a density of 2.5×10^5 cells cm^{-2}. The cells were stimulated with 0.2 µg ml^{-1} doxycyline for in 2 ml E8 36 h. NOGGIN-conditioned E8 medium was then centrifuged to remove cell debris, and supplemented with 1X Knockout-SR, 1X MEM NEAA, 1X GlutaMAX, 1X Insulin/Transferrin/Selenium, 1X Pyruvate, 1X B27 without vitamin A, 1X 2-Mercaptoethanol, and 20 ng ml^{-1} bFGF.

NOGGIN-conditioned medium was added to either the apical or basal compartment of transwell filter cassette before being collected after 36 h for western blotting as described above.

Epithelium membrane integrity was assessed via fluorescent-conjugated 40-kDA Dextran-TxRed/40-kDA Dextran-FITC permeability assay and immuno visualization of an apical meshwork of ZO-1.

QUANTIFICATION AND STATISTICAL ANALYSIS

Image Analysis—Image processing and analysis for endosome co-localization were carried out with the ImageJ software. Following background subtraction, the image was converted to binary, then median filtering was applied. NOGGIN/endosome overlap was obtained via the Image Calculator plugin with the operator “min.” A Z-axis profile was generated for each channel.

$$\%\ \text{NOGGIN co-localizing to an endosome} = \frac{\text{overlap}}{\text{total V5 labeling}} 100\%$$

$$\%\ \text{endosome co-localizing to V5} = \frac{\text{overlap}}{\text{total endosome labeling}} 100\%$$

These operations were applied for all the confocal sections of a confocal stack in each 50 μm × 50 μm region of interest. 4 regions of interest were analyzed per group.

pSMAD1/5 signal propagation analysis: A median filter with a box size of ~2/3 of a nuclear radius was applied to all images to eliminate extreme values while preserving edges. The nuclei of BMP secreting cells were defined by thresholding the strong nuclear marker, which is easily done since their average density is 1:200. The nuclear masks were all verified visually. A distance function was computed for each pixel giving its location to the nearest pixel in a BMP secreting cell. The pSMAD1 signal was averaged in distance bins ~ nuclear radius, with an additional constraint that pixels within the bin distance from the image boundaries were excluded. The first bin included all pixels within the nuclei of the secreting cells (distance 0), which were generally higher than the surroundings. A background level of pSMAD1 was defined by the lowest 10% of pixels that are simultaneously fall within the highest 75% of the DAPI intensity range. (The nuclei occupy at least 50% of the image area.) The background pSMAD1 level was computed and subtracted separately for each image, but were generally consistent across all images to about 10–20%.

Statistical Methods—All values are reported as the mean where the error bars represent SD or SEM, as described in the figure's legend. For all experiments *p<0.05, **p<0.01, ***p<0.001. Statistical quantification was performed on the statistical graphing software GraphPad Prism v9.0.

Supplementary Material

Refer to Web version on PubMed Central for supplementary material.

ACKNOWLEDGMENTS

This work was funded by the National Institutes of Health R01 HD080699 and R01 GM101653.

T.P.E was supported by the National Science Foundation Graduate Research Fellowship under Award No. 1946429.

We thank E. Rodriguez-Boulan for discussions about endosomal trafficking.

REFERENCES

ABASSI YA, XI B, ZHANG W, YE P, KIRSTEIN SL, GAYLORD MR, FEINSTEIN SC, WANG X & XU X 2009. Kinetic cell-based morphological screening: prediction of mechanism of compound action and off-target effects. Chem Biol, 16, 712–23. [PubMed: 19635408]

AKIYAMA T, ISHIDA J, NAKAGAWA S, OGAWARA H, WATANABE S, ITOH N, SHIBUYA M & FUKAMI Y 1987. Genistein, a specific inhibitor of tyrosine-specific protein kinases. J Biol Chem, 262, 5592–5. [PubMed: 3106339]

AOKI T, NOMURA R & FUJIMOTO T 1999. Tyrosine phosphorylation of caveolin-1 in the endothelium. Exp Cell Res, 253, 629–36. [PubMed: 10585286]

ARNOLD SJ & ROBERTSON EJ 2009. Making a commitment: cell lineage allocation and axis patterning in the early mouse embryo. Nat Rev Mol Cell Biol, 10, 91–103. [PubMed: 19129791]

BALLERMANN BJ, DARDIK A, ENG E & LIU A 1998. Shear stress and the endothelium. Kidney Int Suppl, 67, S100–8. [PubMed: 9736263]

BRENT AE & TABIN CJ 2002. Developmental regulation of somite derivatives: muscle, cartilage and tendon. Curr Opin Genet Dev, 12, 548–57. [PubMed: 12200160]

BROWN PS, WANG E, AROETI B, CHAPIN SJ, MOSTOV KE & DUNN KW 2000. Definition of distinct compartments in polarized Madin-Darby canine kidney (MDCK) cells for membrane-volume sorting, polarized sorting and apical recycling. Traffic, 1, 124–40. [PubMed: 11208093]

BRUNNER P, HASTAR N, KAEHLER C, BURDZINSKI W, JATZLAU J & KNAUS P 2020. AMOT130 drives BMP-SMAD signaling at the apical membrane in polarized cells. Mol Biol Cell, 31, 118–130. [PubMed: 31800378]

CRESAWN KO, POTTER BA, OZTAN A, GUERRIERO CJ, IHRKE G, GOLDENRING JR, APODACA G & WEISZ OA 2007. Differential involvement of endocytic compartments in the biosynthetic traffic of apical proteins. EMBO J, 26, 3737–48. [PubMed: 17673908]

CRICK F 1970. Diffusion in Embryogenesis. Nature, 225, 420-&. [PubMed: 5411117]

CUI Y, HACKENMILLER R, BERG L, JEAN F, NAKAYAMA T, THOMAS G & CHRISTIAN JL 2001. The activity and signaling range of mature BMP-4 is regulated by sequential cleavage at two sites within the prodomain of the precursor. Genes Dev, 15, 2797–802. [PubMed: 11691831]

DEGNIN C, JEAN F, THOMAS G & CHRISTIAN JL 2004. Cleavages within the prodomain direct intracellular trafficking and degradation of mature bone morphogenetic protein-4. Mol Biol Cell, 15, 5012–20. [PubMed: 15356272]

DELVAUX M, BASTIE MJ, CHENTOUFI J, CRAGOE EJ JR., VAYSSE N & RIBET A 1990. Amiloride and analogues inhibit Na(+)–H+ exchange and cell proliferation in AR42J pancreatic cell line. Am J Physiol, 259, G842–9. [PubMed: 2173418]

DUTTA D & DONALDSON JG 2012. Search for inhibitors of endocytosis: Intended specificity and unintended consequences. Cell Logist, 2, 203–208. [PubMed: 23538558]

DUTTA D, WILLIAMSON CD, COLE NB & DONALDSON JG 2012. Pitstop 2 is a potent inhibitor of clathrin-independent endocytosis. PLoS One, 7, e45799. [PubMed: 23029248]

ETOC F, METZGER J, RUZO A, KIRST C, YONEY A, OZAIR MZ, BRIVANLOU AH & SIGGIA ED 2016. A Balance between Secreted Inhibitors and Edge Sensing Controls Gastruloid Self-Organization. Dev Cell, 39, 302–315. [PubMed: 27746044]

FUJIMOTO LM, ROTH R, HEUSER JE & SCHMID SL 2000. Actin assembly plays a variable, but not obligatory role in receptor-mediated endocytosis in mammalian cells. Traffic, 1, 161–71. [PubMed: 11208096]

GILMOUR D, REMBOLD M & LEPTIN M 2017. From morphogen to morphogenesis and back. Nature, 541, 311–320. [PubMed: 28102269]

HAMM-ALVAREZ SF, SONEE M, LORAN-GOSS K & SHEN WC 1996. Paclitaxel and nocodazole differentially alter endocytosis in cultured cells. Pharm Res, 13, 1647–56. [PubMed: 8956329]

HARASZTOSI C, KLENSKE E, BADUM S, HARASZTOSI E & GUMMER AW 2018. Double fluorescent labelling of a bipolar epithelial cell in vitro: The outer hair cell. J Neurosci Methods, 293, 310–320. [PubMed: 29054590]

HARTUNG A, BITTON-WORMS K, RECHTMAN MM, WENZEL V, BOERGERMANN JH, HASSEL S, HENIS YI & KNAUS P 2006. Different routes of bone morphogenic protein (BMP) receptor endocytosis influence BMP signaling. Mol Cell Biol, 26, 7791–805. [PubMed: 16923969]

HIDALGO DAH,Z; ROMANOVA-MICHAELIDES M; GONZÁLEZ-GAITÁN M; JÜLICHER F 2019. Dynamic modes of morphogen transport. arXiv, 1909.13280.

HOEBEKE J, VAN NIJEN G & DE BRABANDER M 1976. Interaction of oncodazole (R 17934), a new antitumoral drug, with rat brain tubulin. Biochem Biophys Res Commun, 69, 319–24. [PubMed: 1267789]

HUANG JJ, WANG YJ, ZHANG M, ZHANG P, LIANG H, BAI HJ, YU XJ & YANG HT 2017. Functional expression of the Ca(2+) signaling machinery in human embryonic stem cells. Acta Pharmacol Sin, 38, 1663–1672. [PubMed: 28713161]

IVANOV AI 2008. Pharmacological inhibition of endocytic pathways: is it specific enough to be useful? Methods Mol Biol, 440, 15–33. [PubMed: 18369934]

JACKMAN MR, SHURETY W, ELLIS JA & LUZIO JP 1994. Inhibition of apical but not basolateral endocytosis of ricin and folate in Caco-2 cells by cytochalasin D. J Cell Sci, 107 (Pt 9), 2547–56. [PubMed: 7844170]

KNIGHT A, HUGHSON E, HOPKINS CR & CUTLER DF 1995. Membrane protein trafficking through the common apical endosome compartment of polarized Caco-2 cells. Mol Biol Cell, 6, 597–610. [PubMed: 7545032]

KOIVUSALO M, WELCH C, HAYASHI H, SCOTT CC, KIM M, ALEXANDER T, TOURET N, HAHN KM & GRINSTEIN S 2010. Amiloride inhibits macropinocytosis by lowering submembranous pH and preventing Rac1 and Cdc42 signaling. J Cell Biol, 188, 547–63. [PubMed: 20156964]

KORNBERG TB 2017. Distributing signaling proteins in space and time: the province of cytonemes. Curr Opin Genet Dev, 45, 22–27. [PubMed: 28242479]

LACOSTE A, BERENSHTEYN F & BRIVANLOU AH 2009. An efficient and reversible transposable system for gene delivery and lineage-specific differentiation in human embryonic stem cells. Cell Stem Cell, 5, 332–42. [PubMed: 19733544]

LAGANA A, VADNAIS J, LE PU, NGUYEN TN, LAPRADE R, NABI IR & NOEL J 2000. Regulation of the formation of tumor cell pseudopodia by the Na(+)/H(+) exchanger NHE1. J Cell Sci, 113 (Pt 20), 3649–62. [PubMed: 11017880]

LAPIERRE LA, DUCHARME NA, DRAKE KR, GOLDENRING JR & KENWORTHY AK 2012. Coordinated regulation of caveolin-1 and Rab11a in apical recycling compartments of polarized epithelial cells. Exp Cell Res, 318, 103–13. [PubMed: 22036648]

LI L, WAN T, WAN M, LIU B, CHENG R & ZHANG R 2015. The effect of the size of fluorescent dextran on its endocytic pathway. Cell Biol Int, 39, 531–9. [PubMed: 25623938]

LINSTEDT AD & HAURI HP 1993. Giantin, a novel conserved Golgi membrane protein containing a cytoplasmic domain of at least 350 kDa. Mol Biol Cell, 4, 679–93. [PubMed: 7691276]

MARTYN I, BRIVANLOU AH & SIGGIA ED 2019. A wave of WNT signaling balanced by secreted inhibitors controls primitive streak formation in micropattern colonies of human embryonic stem cells. Development, 146.

MATOS I, ASARE A, LEVORSE J, OUSPENSKAIA T, DE LA CRUZ-RACELIS J, SCHUHMACHER LN & FUCHS E 2020. Progenitors oppositely polarize WNT activators and inhibitors to orchestrate tissue development. Elife, 9.

MAYER TU, KAPOOR TM, HAGGARTY SJ, KING RW, SCHREIBER SL & MITCHISON TJ 1999. Small molecule inhibitor of mitotic spindle bipolarity identified in a phenotype-based screen. Science, 286, 971–4. [PubMed: 10542155]

MCCLUSKEY A, DANIEL JA, HADZIC G, CHAU N, CLAYTON EL, MARIANA A, WHITING A, GORGANI NN, LLOYD J, QUAN A, MOSHKANBARYANS L, KRISHNAN S, PERERA S, CHIRCOP M, VON KLEIST L, MCGEACHIE AB, HOWES MT, PARTON RG, CAMPBELL M, SAKOFF JA, WANG X, SUN JY, ROBERTSON MJ, DEANE FM, NGUYEN TH, MEUNIER FA, COUSIN MA & ROBINSON PJ 2013. Building a better dynasore: the dyngo compounds potently inhibit dynamin and endocytosis. Traffic, 14, 1272–89. [PubMed: 24025110]

MCMAHON JA, TAKADA S, ZIMMERMAN LB, FAN CM, HARLAND RM & MCMAHON AP 1998. Noggin-mediated antagonism of BMP signaling is required for growth and patterning of the neural tube and somite. Genes Dev, 12, 1438–52. [PubMed: 9585504]

MORGAN TH 1901. Regeneration in the egg, embryo, and adult. American Naturalist, 35, 949–973.

MULLER P, ROGERS KW, YU SR, BRAND M & SCHIER AF 2013. Morphogen transport. Development, 140, 1621–38. [PubMed: 23533171]

NABI IR & LE PU 2003. Caveolae/raft-dependent endocytosis. J Cell Biol, 161, 673–7. [PubMed: 12771123]

NALLET-STAUB F, YIN X, GILBERT C, MARSAUD V, BEN MIMOUN S, JAVELAUD D, LEOF EB & MAUVIEL A 2015. Cell density sensing alters TGF-beta signaling in a cell-type-specific manner, independent from Hippo pathway activation. Dev Cell, 32, 640–51. [PubMed: 25758862]

O'RAHILLY R & MULLER F 2010. Developmental stages in human embryos: revised and new measurements. Cells Tissues Organs, 192, 73–84. [PubMed: 20185898]

ODORIZZI G, PEARSE A, DOMINGO D, TROWBRIDGE IS & HOPKINS CR 1996. Apical and basolateral endosomes of MDCK cells are interconnected and contain a polarized sorting mechanism. J Cell Biol, 135, 139–52. [PubMed: 8858169]

OHKAWARA B, IEMURA S, TEN DIJKE P & UENO N 2002. Action range of BMP is defined by its N-terminal basic amino acid core. Curr Biol, 12, 205–9. [PubMed: 11839272]

PAARMANN P, DORPHOLZ G, FIEBIG J, AMSALEM AR, EHRLICH M, HENIS YI, MULLER T & KNAUS P 2016. Dynamin-dependent endocytosis of Bone Morphogenetic Protein2 (BMP2) and its receptors is dispensable for the initiation of Smad signaling. Int J Biochem Cell Biol, 76, 51–63. [PubMed: 27113717]

PAINE-SAUNDERS S, VIVIANO BL, ECONOMIDES AN & SAUNDERS S 2002. Heparan sulfate proteoglycans retain Noggin at the cell surface: a potential mechanism for shaping bone morphogenetic protein gradients. J Biol Chem, 277, 2089–96. [PubMed: 11706034]

PARK RJ, SHEN H, LIU L, LIU X, FERGUSON SM & DE CAMILLI P 2013. Dynamin triple knockout cells reveal off target effects of commonly used dynamin inhibitors. J Cell Sci, 126, 5305–12. [PubMed: 24046449]

PEREZ BAY AE, SCHREINER R, BENEDICTO I, PAZ MARZOLO M, BANFELDER J, WEINSTEIN AM & RODRIGUEZ-BOULAN EJ 2016. The fast-recycling receptor Megalin defines the apical recycling pathway of epithelial cells. Nat Commun, 7, 11550. [PubMed: 27180806]

RIDER CC & MULLOY B 2017. Heparin, Heparan Sulphate and the TGF-beta Cytokine Superfamily. Molecules, 22.

RODRIGUEZ-BOULAN E, KREITZER G & MUSCH A 2005. Organization of vesicular trafficking in epithelia. Nat Rev Mol Cell Biol, 6, 233–47. [PubMed: 15738988]

RODRIGUEZ-BOULAN E & MACARA IG 2014. Organization and execution of the epithelial polarity programme. Nat Rev Mol Cell Biol, 15, 225–42. [PubMed: 24651541]

ROGERS KW & SCHIER AF 2011. Morphogen Gradients: From Generation to Interpretation. Annual Review of Cell and Developmental Biology, Vol 27, 27, 377–407.

SAMPATH P & POLLARD TD 1991. Effects of cytochalasin, phalloidin, and pH on the elongation of actin filaments. Biochemistry, 30, 1973–80. [PubMed: 1899622]

SCHLIWA M 1982. Action of cytochalasin D on cytoskeletal networks. J Cell Biol, 92, 79–91. [PubMed: 7199055]

SHAHBAZI MN 2020. Mechanisms of human embryo development: from cell fate to tissue shape and back. Development, 147.

SHAHBAZI MN & ZERNICKA-GOETZ M 2018. Deconstructing and reconstructing the mouse and human early embryo. Nat Cell Biol, 20, 878–887. [PubMed: 30038253]

SHEFF DR, DARO EA, HULL M & MELLMAN I 1999. The receptor recycling pathway contains two distinct populations of early endosomes with different sorting functions. J Cell Biol, 145, 123–39. [PubMed: 10189373]

SIMONSEN A, LIPPE R, CHRISTOFORIDIS S, GAULLIER JM, BRECH A, CALLAGHAN J, TOH BH, MURPHY C, ZERIAL M & STENMARK H 1998. EEA1 links PI(3)K function to Rab5 regulation of endosome fusion. Nature, 394, 494–8. [PubMed: 9697774]

SIMUNOVIC M, METZGER JJ, ETOC F, YONEY A, RUZO A, MARTYN I, CROFT G, YOU DS, BRIVANLOU AH & SIGGIA ED 2019. A 3D model of a human epiblast reveals BMP4-driven symmetry breaking. Nat Cell Biol, 21, 900–910. [PubMed: 31263269]

SMITH WC & HARLAND RM 1992. Expression cloning of noggin, a new dorsalizing factor localized to the Spemann organizer in Xenopus embryos. Cell, 70, 829–40. [PubMed: 1339313]

SORRE B, WARMFLASH A, BRIVANLOU AH & SIGGIA ED 2014. Encoding of temporal signals by the TGF-beta pathway and implications for embryonic patterning. Dev Cell, 30, 334–42. [PubMed: 25065773]

STUMPF HF 1966. Mechanism by Which Cells Estimate Their Location within Body. Nature, 212, 430-&. [PubMed: 5970169]

SUBTIL A & DAUTRY-VARSAT A 1997. Microtubule depolymerization inhibits clathrin coated-pit internalization in non-adherent cell lines while interleukin 2 endocytosis is not affected. J Cell Sci, 110 (Pt 19), 2441–7. [PubMed: 9410882]

TYSER RCVM,E; NAKANOH S; VALLIER L; SCIALDONE A; SRINIVAS A 2020. A spatially resolved single cell atlas of human gastrulation. bioRxiv.

VASQUEZ RJ, HOWELL B, YVON AM, WADSWORTH P & CASSIMERIS L 1997. Nanomolar concentrations of nocodazole alter microtubule dynamic instability in vivo and in vitro. Mol Biol Cell, 8, 973–85. [PubMed: 9201709]

VERCAUTEREN D, VANDENBROUCKE RE, JONES AT, REJMAN J, DEMEESTER J, DE SMEDT SC, SANDERS NN & BRAECKMANS K 2010. The use of inhibitors to study endocytic pathways of gene carriers: optimization and pitfalls. Mol Ther, 18, 561–9. [PubMed: 20010917]

VON KLEIST L, STAHLSCHMIDT W, BULUT H, GROMOVA K, PUCHKOV D, ROBERTSON MJ, MACGREGOR KA, TOMILIN N, PECHSTEIN A, CHAU N, CHIRCOP M, SAKOFF J, VON KRIES JP, SAENGER W, KRAUSSLICH HG, SHUPLIAKOV O, ROBINSON PJ, MCCLUSKEY A & HAUCKE V 2011. Role of the clathrin terminal domain in regulating coated pit dynamics revealed by small molecule inhibition. Cell, 146, 471–84. [PubMed: 21816279]

WANG LH, ROTHBERG KG & ANDERSON RG 1993. Mis-assembly of clathrin lattices on endosomes reveals a regulatory switch for coated pit formation. J Cell Biol, 123, 1107–17. [PubMed: 8245121]

WARMFLASH A, ARDUINI BL & BRIVANLOU AH 2012. The molecular circuitry underlying pluripotency in embryonic stem cells. Wiley Interdiscip Rev Syst Biol Med, 4, 443–56. [PubMed: 22761038]

WARTLICK O, JULICHER F & GONZALEZ-GAITAN M 2014. Growth control by a moving morphogen gradient during Drosophila eye development. Development, 141, 1884–93. [PubMed: 24757005]

WARTLICK O, KICHEVA A & GONZALEZ-GAITAN M 2009. Morphogen gradient formation. Cold Spring Harb Perspect Biol, 1, a001255. [PubMed: 20066104]

WILLOX AK, SAHRAOUI YM & ROYLE SJ 2014. Non-specificity of Pitstop 2 in clathrin-mediated endocytosis. Biol Open, 3, 326–31. [PubMed: 24705016]

WITTE L, LINNEMANNSTONS K, SCHMIDT K, HONEMANN-CAPITO M, GRAWE F, WODARZ A & GROSS JC 2020. The kinesin motor Klp98A mediates apical to basal Wg transport. Development, 147.

YAMAZAKI Y, PALMER L, ALEXANDRE C, KAKUGAWA S, BECKETT K, GAUGUE I, PALMER RH & VINCENT JP 2016. Godzilla-dependent transcytosis promotes Wingless signalling in Drosophila wing imaginal discs. Nat Cell Biol, 18, 451–7. [PubMed: 26974662]

YAN D & LIN X 2009. Shaping morphogen gradients by proteoglycans. Cold Spring Harb Perspect Biol, 1, a002493. [PubMed: 20066107]

YAO CK, LIU YT, LEE IC, WANG YT & WU PY 2017. A Ca2+ channel differentially regulates Clathrin-mediated and activity-dependent bulk endocytosis. PLoS Biol, 15, e2000931. [PubMed: 28414717]

YBOT-GONZALEZ P, SAVERY D, GERRELLI D, SIGNORE M, MITCHELL CE, FAUX CH, GREENE ND & COPP AJ 2007. Convergent extension, planar-cell-polarity signalling and initiation of mouse neural tube closure. Development, 134, 789–99. [PubMed: 17229766]

YONEY A, ETOC F, RUZO A, CARROLL T, METZGER JJ, MARTYN I, LI S, KIRST C, SIGGIA ED & BRIVANLOU AH 2018. WNT signaling memory is required for ACTIVIN to function as a morphogen in human gastruloids. Elife, 7.

ZHANG Z, ZWICK S, LOEW E, GRIMLEY JS & RAMANATHAN S 2019. Mouse embryo geometry drives formation of robust signaling gradients through receptor localization. Nat Commun, 10, 4516. [PubMed: 31586065]

ZIMMERMAN LB, DE JESUS-ESCOBAR JM & HARLAND RM 1996. The Spemann organizer signal noggin binds and inactivates bone morphogenetic protein 4. Cell, 86, 599–606. [PubMed: 8752214]

Highlights

- NOGGIN and BMP4 are secreted to separate, opposite extracellular spaces
- Apically-applied NOGGIN can inhibit basally-applied BMP4
- NOGGIN undergoes apical-to-basal transcytosis
- The endocytotic route involved in NOGGIN trafficking is characterized

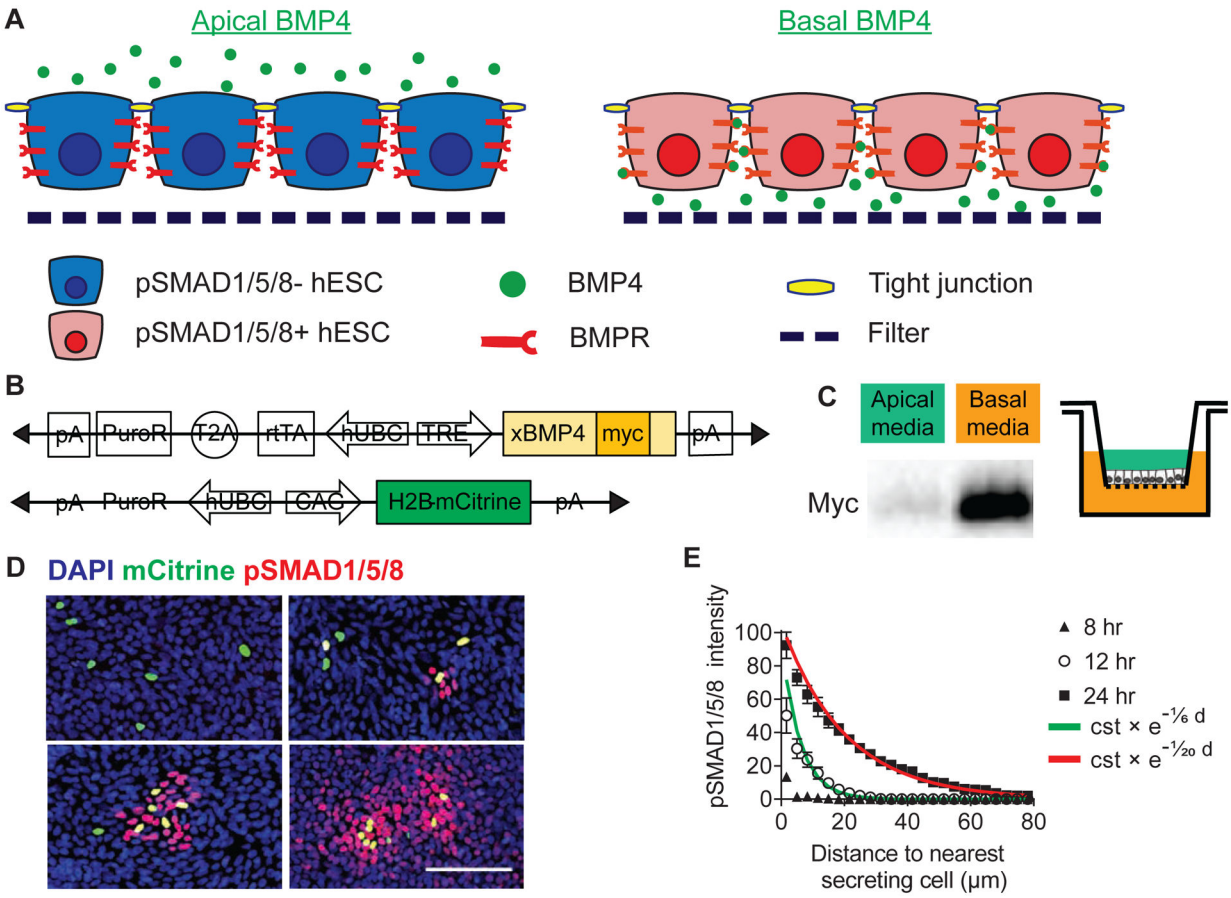

Figure 1: BMP4 is secreted basally and spreads from a local source.

(A) Schematics of polarized hESC epithelium. BMPR localization restricts hESC response to BMP4 to the basolateral domain. (B) Schematics of the doxycycline-inducible constructs for the generation of the xBMP4-overexpressing hESC line. A Myc tag was inserted near the C-terminal of the coding sequence of the precursor protein (N-terminal of the mature protein) (Degnin et al., 2004, Cui et al., 2001), so that both precursor and mature forms of exogenously expressed BMP4 can be detected by the Myc epitope. A constitutive mCitrine nuclear reporter was added subsequently. (C) BMP4 was secreted to the basolateral media. TRE::xBMP4-myc hESCs were cultured to form a tight epithelium on filter and induced to produce BMP4. After 24 hrs, culture media collected from the apical (green) or basal (orange) chambers were analyzed with Western blot. (D) BMP4 signaling propagated in the epithelium as a function of time. pSMAD1/5/8 signaling originated from TRE::BMP4-myc; CAG::H2B-mCitrine cells and propagated to adjacent cells. TRE::xBMP4-myc; CAG::H2B-mCitrine were diluted in wildtype (WT) hESCs (ratio 1:200) and induced to produce BMP4. pSMAD1/5/8 signal intensity was used as a read-out for BMP4 reception in time-course analysis. Scale bar = 100 μm. (E) Quantification of BMP4 signal propagation as a function of time. Exponential curves were fitted to the datapoints. The exponential function is described by the constant “cst” which is the prefactor of the exponential function and the spreading length (in μm) which characterizes the function’s rate of decay. Error bars = SEM (standard error of mean). See also Supp Fig 2.

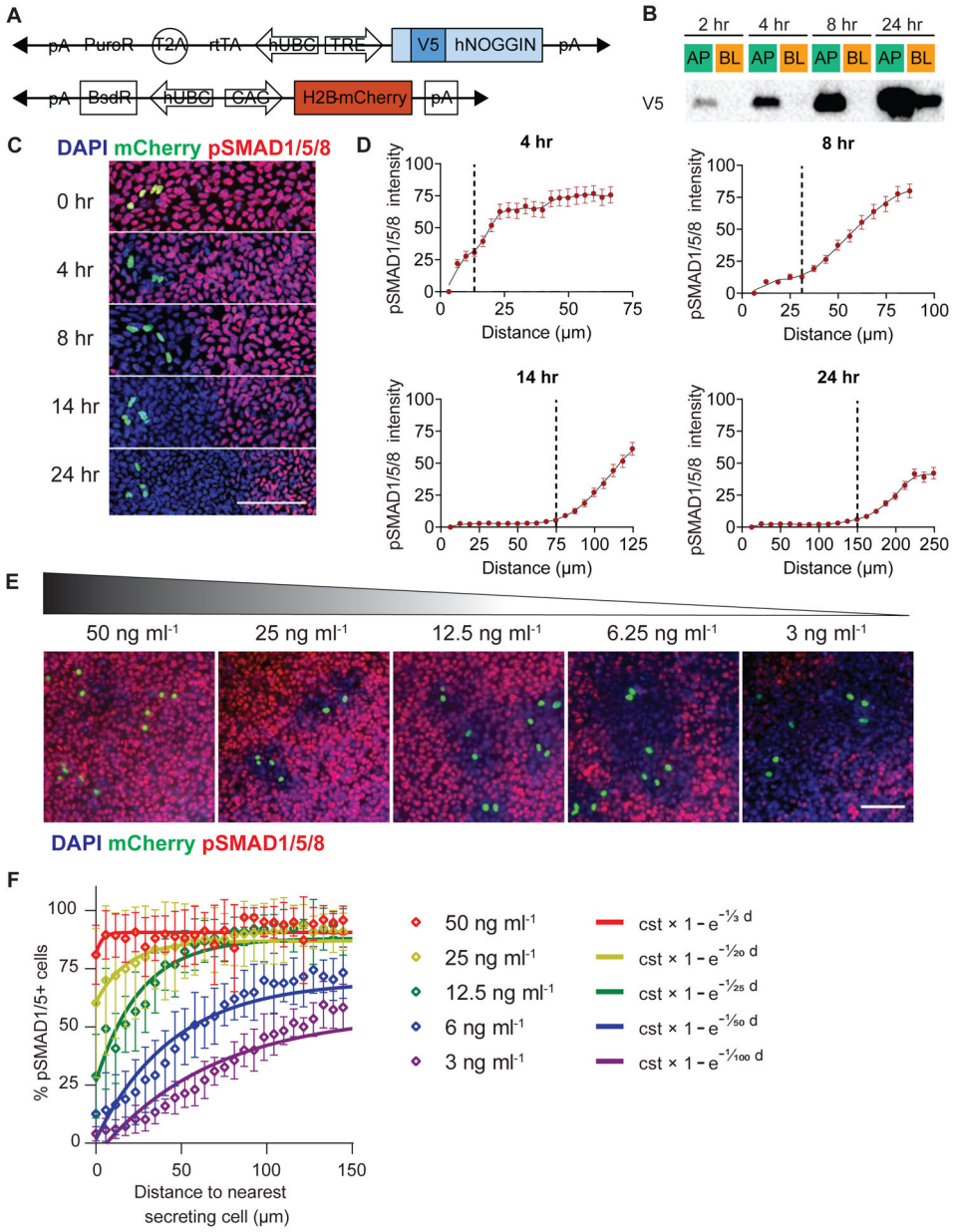

Figure 2: NOGGIN was secreted apically. Apically-delivered recombinant NOGGIN inhibited basal BMP4.

(A) Schematics of the doxycycline-inducible constructs for the generation of the hNOGGIN-overexpressing hESC line. A V5 tag was inserted at the N-terminal of the protein-coding sequence (Etoc et al., 2016). A constitutive mCherry nuclear reporter was subsequent added. (B) NOGGIN was secreted to the apical media. TRE::V5-NOGGIN hESCs were cultured on filters to form confluent epithelia and induced to produce NOGGIN for 2, 4, 8, or 24 hrs. Media collected from the apical (AP) or basolateral (BL) chambers were collected and analyzed with Western blot. (C) The range of NOGGIN's inhibitory effects extended as a function of time. TRE::V5-NOGGIN hESCs; CAG::H2B-mCherry were diluted in a background of WT hESCs (ratio 1:200) and induced to secret NOGGIN for the specified times. Then, BMP4 (10 ng ml^{-1}) was applied basally for 1 hr. pSMAD1/5/8 labeling

demarcated the range of NOGGIN inhibition. The yellow cells one seen in the panel at 0 hrs are NOGGIN secreting cells (nuclear label green) that are pSMAD-positive (red). Scale bars = 100 μm. (D) Quantification of NOGGIN inhibitory range as a function of time. The black vertical dashed lines indicate the point where the local slope of the fit changes (maximum of second derivative). Error bars = SEM. (E) NOGGIN inhibitory range as a function of BMP4 concentration. TRE::V5-NOGGIN hESCs were diluted in a background of WT hESCs (ratio 1:200) and induced to secret NOGGIN (8 hrs). Then, different concentrations of recombinant BMP4 was applied basally for 1 hr. The range of NOGGIN inhibition was inversely correlated with the concentration of BMP4. Scale bars = 100 μm. (F) Quantification of NOGGIN's efficacy in inhibiting pSMAD1/5/8 BMP4 concentration as a function of BMP4 concentration. Exponential curves were fitted to the datapoints. The exponential function is described by the constant "cst" which is the prefactor of the exponential function and the exclusion length (in μm). Error bars = SEM. See also Supp Fig 3.

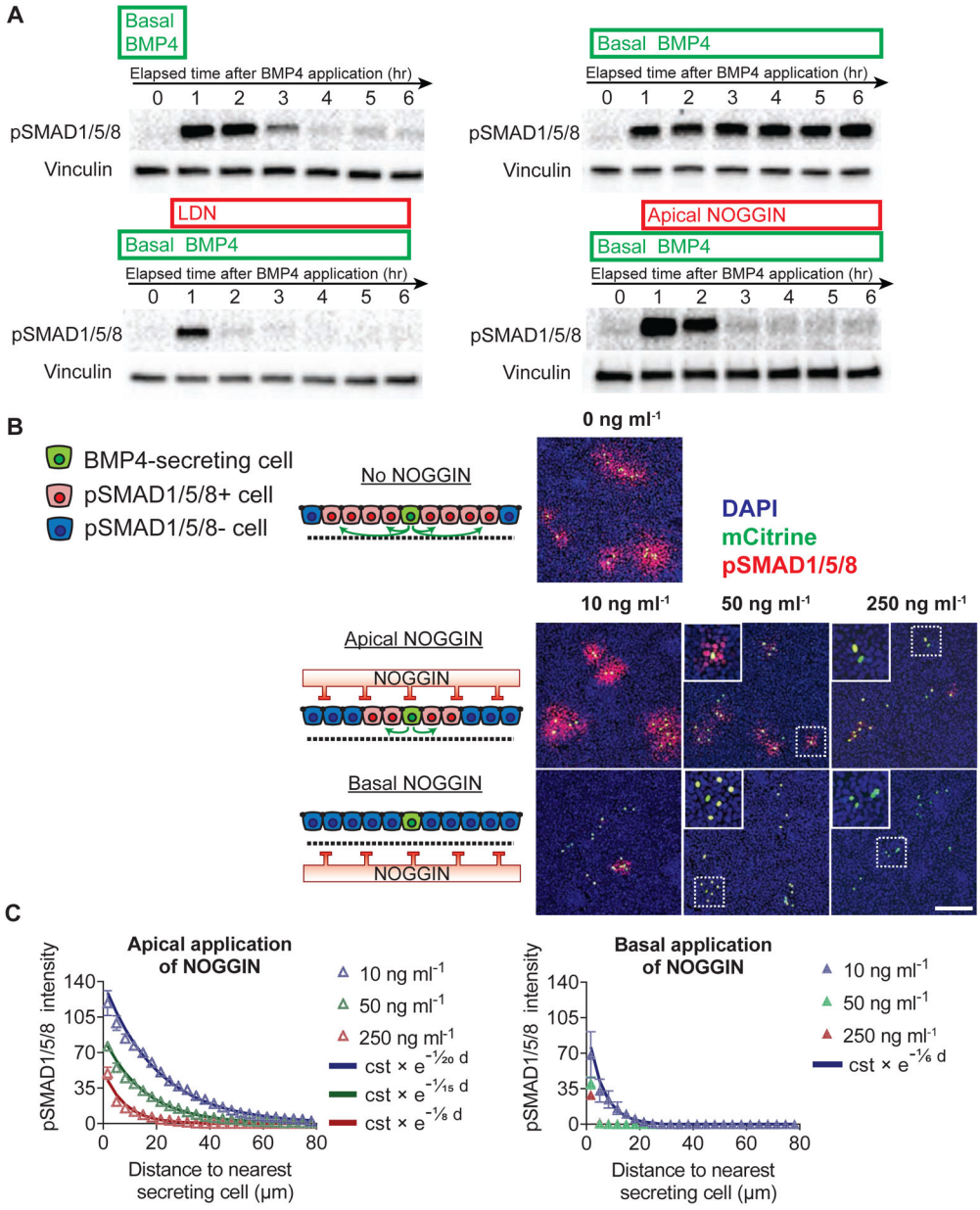

Figure 3: Secreted NOGGIN inhibited BMP4 signaling in the epithelium.

(A) Apically-applied recombinant hNOGGIN inhibited pSMAD1/5/8 induced by recombinant BMP4. Top row: 1-hr pulse (left) or sustained (right) application of recombinant BMP4 (10 ng ml^{-1}) elicited pSMAD1/5/8 response. Bottom row: This pSMAD1/5/8 response was rapidly inhibited by LDN (a BMP inhibitor that blocks the transcriptional activity of BMPR1 receptors ALK2 and ALK3) (0.1 μM) (left) or apically-applied recombinant hNOGGIN (250 ng ml^{-1}) (right). Horizontal axes indicate elapsed time following BMP4 application. (B) Apically-applied recombinant hNOGGIN inhibited BMP4 signaling within the epithelium. TRE::xBMP4-myc hESCs; CAG::H2B-mCitrine were mixed with WT hESCs (ratio 1:200) and induced to produce BMP4 for 22 hr. Different concentrations of recombinant hNOGGIN was added to the layer apically or basally for 2

hr. 250 ng ml^{-1} NOGGIN efficiently inhibited autonomous pSMAD1/5/8 in BMP4-secreting cells. Scale bar = 100 μm. (C) Quantification of inhibitory efficacies of apically- and basally-applied recombinant hNOGGIN. Exponential curves were fitted to the datapoints. The exponential function is described by the constant “cst” which is the prefactor of the exponent function and the spreading length (in μm) which characterizes the function’s rate of decay. Error bars = SEM. See also Supp Fig 3.

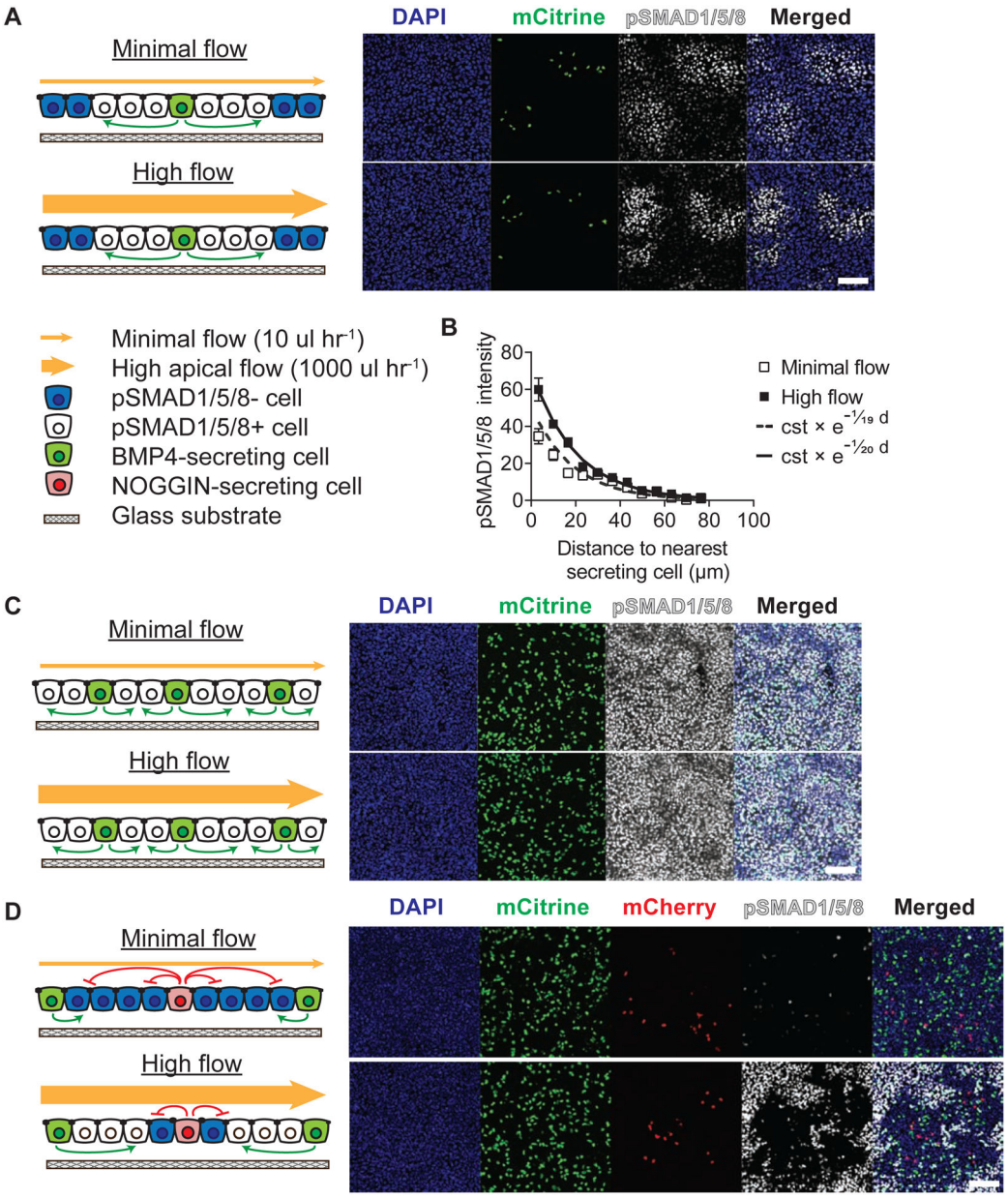

Figure 4: Apical flow perturbed NOGGIN inhibition in epithelium.

(A) Apical flow did not affect BMP4 signal propagation. A mixture of TRE::BMP4-myc; CAG::H2B-mCitrine and WT hESCs (ratio 1:500) was cultured overnight in microfluidic chambers. For all experiments in this figure, cells were induced to produce BMP4 under minimal (10 μl hr^{-1}) or high apical flow (1000 μl hr^{-1}) conditions for 6 hrs, before being stained for pSMAD1/5/8. (B) Quantification of the effect of apical flow on BMP4 signal propagation. Exponential curves were fitted to the datapoints. The exponential function is described by the constant "cst" which is the prefactor of the exponent function and the spreading length (in μm) which characterizes the function's rate of decay. Error bars = SEM. (C) Epithelia with a 1:10 ratio of BMP4 secreting to naive cells exhibited homogenous pSMAD1/5/8 activation under both minimal and high flow conditions. (D) High apical

flow perturbed NOGGIN inhibition. A mixture of TRE::V5-NOGGIN; CAG::H2B-mCherry, TRE::BMP4-myc; CAG::H2B-mCtrine, and WT hESCs (ratio 1:50:500) was cultured in microfluidic chambers. High apical flow perturbed NOGGIN's long-range inhibitory effects. Error bars = SEM. Scale bars = 100 μm. See also Supp Figs 4, 5.

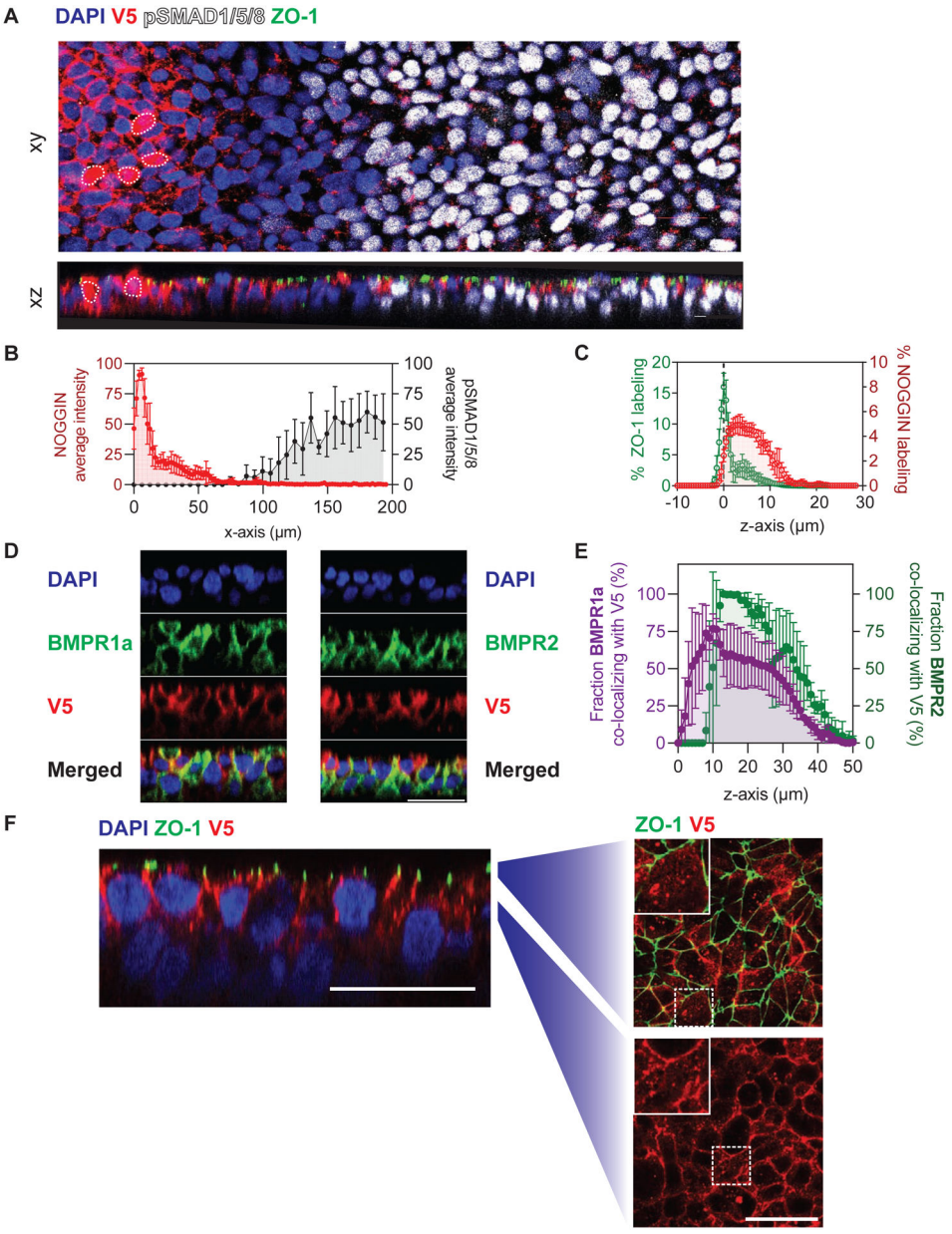

Figure 5: NOGGIN was detected laterally beneath tight junctions and as puncta in receiving cells.

(A) NOGGIN spread to neighboring cells away from secreting cells. A small number of TRE::V5-NOGGIN cells were co-cultured with WT hESCs on filter. Cells were induced to produce NOGGIN for 8 hrs before BMP4 (10 ng ml^{-1}) was applied basally for 1 hr. NOGGIN immunolabeling was done with α-V5 antibodies. White dashed outlines indicate NOGGIN-secreting cells. Top (xy): confocal image of the epithelium through a single z-plane. Bottom (xz): sagittal (z-plane) view of the same epithelium. Scale bars = 25 μm. (B) Quantification of NOGGIN and pSMAD1/5/8 average pixel intensity profiles relative to each other along the x-axis. (The peak of NOGGIN intensity correlates with the location of a NOGGIN-secreting cell.) As NOGGIN intensity dropped off, pSMAD1/5/8 intensity increased. Error bars = SD. (C) Quantification of NOGGIN distribution along

the z-axis with respect to ZO-1. NOGGIN localized at and below the level of tight junctions. Error bars = SD. (D) Sagittal (z-plane) view showing NOGGIN co-localizing with BMPR1a and BMPR2. TRE::V5-NOGGIN cells were co-cultured with TRE::BMPR1A-Myc or TRE::BMPR2-HA hESCs on filter (ratio 1:100). Cells were induced to express NOGGIN and BMPR1A/BMPR2 for 24 hrs. BMPR1A and BMPR2 labeling was detected by α-Myc antibodies and α-HA antibodies, respectively. Subsequently, NOGGIN-BMPR co-localization was analyzed in cells at least 5-cell-diameter away from NOGGIN-producing cells. (E) Quantification of the overlap of BMPR1a (left axis, purple) and BMPR2 (right axis, green) with NOGGIN. NOGGIN expression profile was used as a reference to determine the relative z-position. Error bars = SD. (F) Sagittal (z-plane) view showing NOGGIN localization in the epithelium. TRE::V5-NOGGIN cells were co-cultured with WT hESCs (ratio 1:200). Cells were induced to express NOGGIN for 24 hrs. Subsequently, NOGGIN localization was analyzed in cells 5-cell-distance away from NOGGIN-producing cells. Zoom-out panels show transverse views at the corresponding z-position. NOGGIN appeared as puncta (white arrows) at and below tight junction levels. Scale bars = 25 μm.

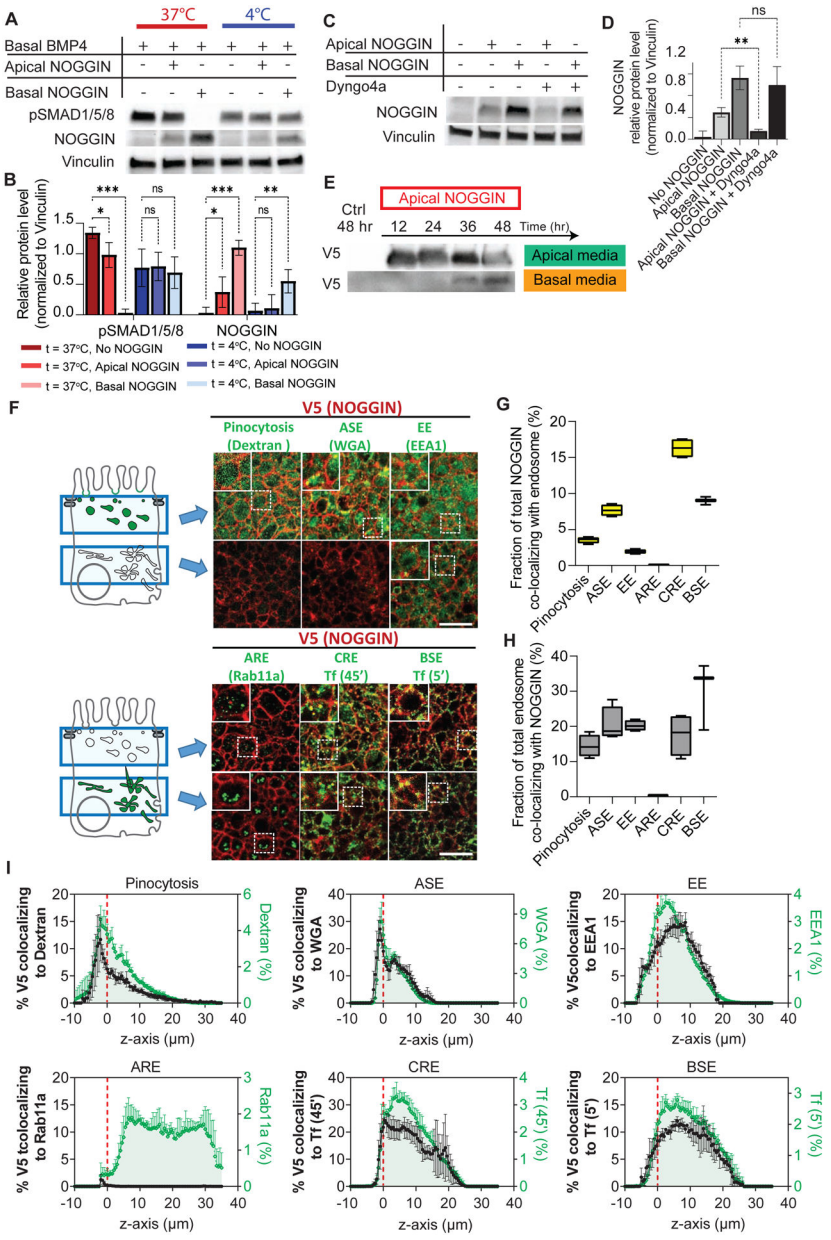

Figure 6: NOGGIN was endocytosed at the apical membrane and transported through endosomal compartments.

(A) NOGGIN inhibitory effects on pSMAD1/5/8 was eliminated at low temperature. WT-RUES2 were stimulated with basal recombinant BMP4 (50 ng ml^{-1}). After 1.5 hr, NOGGIN (250 ng ml^{-1}) was added to the culture either apically or basally, and the culture was kept at 37°C or moved to 4°C. After 2 hrs, cell lysates were collected for Western blot analysis. (B) Quantification of the effect of cold temperature on NOGGIN internalization and pSMAD1/5/8 inhibition. Error bars = SD. Dunnett's multiple comparison statistical tests were performed with n = 6 (ns = not significant; * $p \leq 0.05$; ** $p \leq 0.01$; *** $p \leq 0.001$). (C) NOGGIN was apically internalized via dynamin-dependent endocytosis. Recombinant NOGGIN (250 ng ml^{-1}) was added apically to WT hESCs with or without dynamin inhibitor Dyngo4a (100 mM). After 2 hrs, cell lysates were collected for Western

blot analysis. 2-hr concurrent treatment of Dyngo4a blocked NOGGIN internalization. (D) Quantification of the effect of Dyngo4a in inhibiting NOGGIN internalization. Error bars = SD. Tukey's multiple comparison statistical test was performed with n = 3 (ns = not significant; * $p \leq 0.05$; ** $p \leq 0.01$; *** $p \leq 0.001$). (E) NOGGIN underwent apical-to-basal transcytosis. NOGGIN-V5-conditioned E8 media was applied to the apical compartment for the specified durations. Media from the apical and basal compartments were analyzed with Western blot. The presence of NOGGIN in the basal compartment was detected after 36 hrs. (F) NOGGIN colocalized with various endosomal vesicles. 10-kDA Dextran (10-min apical incubation) labeled pinocytotic vesicles. WGA (wheat germ agglutinin) (10-min apical incubation) labeled ASE (Apical Sorting Endosomes). EEA1 antibodies labeled EE (Early Endosomes). Rab11A antibodies labeled ARE (Apical Recycling Endosomes). Transferrin (45-min basal incubation) (Tf 45') labeled CRE (Common Recycling Endosomes). Transferrin (5 min basal incubation) (Tf 5') labeled BSE (Basal Sorting Endosomes). Left: Schema. Right: Data showing two confocal sections in the apical (top) and supranuclear (bottom) regions. Scale bars = 25 μm. (G) Quantification of the total fraction of NOGGIN co-localizing with each endosomal marker. (H) Quantification of the total fraction of each endosomal marker co-localizing with NOGGIN. For both (G–H), box and whisker plots display minimum, first quartile, median, third quartile, and maximum. (I) Fraction of NOGGIN co-localizing with endocytotic vesicles (left axis, black) at each z-position with respect to the profile of the respective marker (right axis, green) at the corresponding z-position. Datapoints were taken 0.5 μm apart. Fluorescence labeling was binarized. All samples were aligned in the z-axis based on ZO-1 labeling (indicated by red dashed line). Error bars = SD. See also Supp Figs 6, 7 and Supp Table 1.

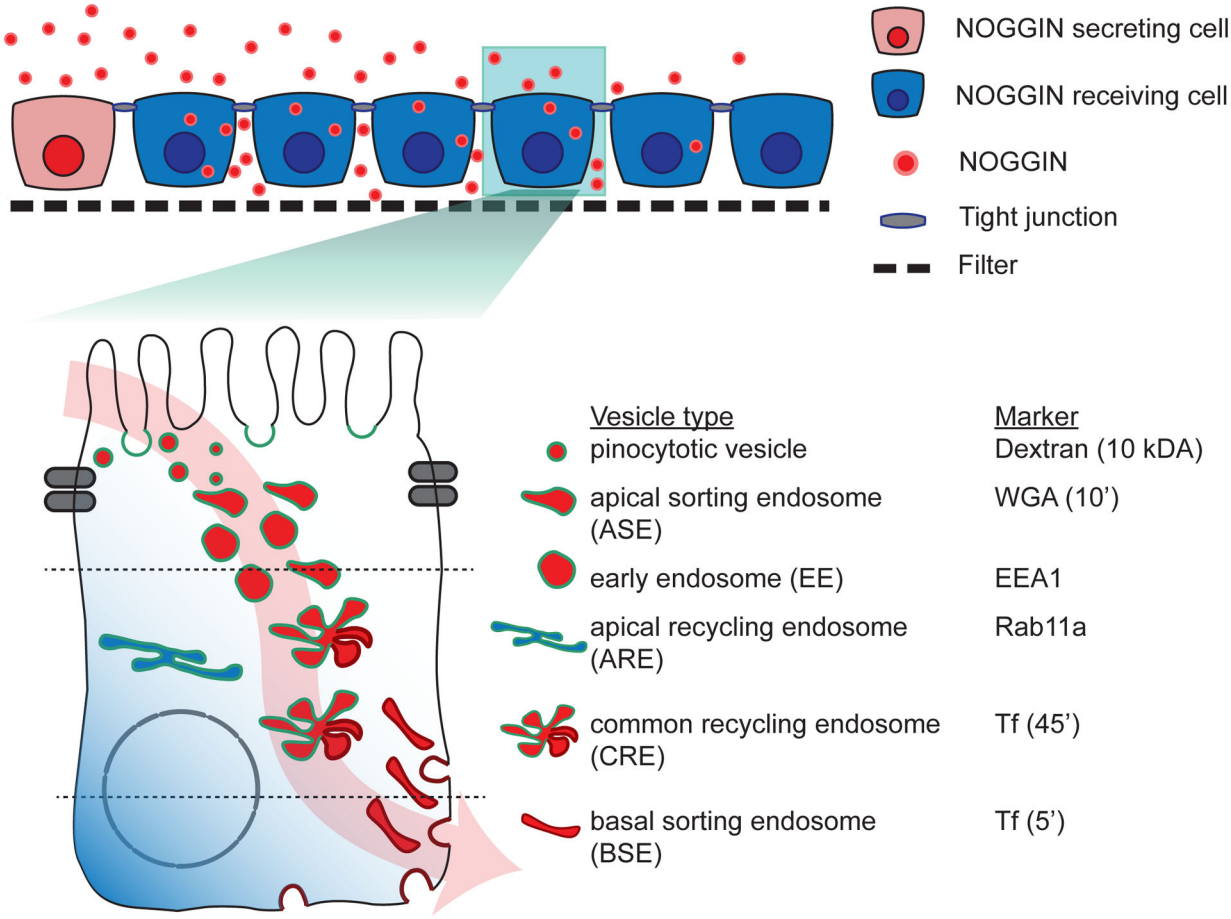

Figure 7: Schematics of transcytosis route through which NOGGIN (red) is trafficked from the apical to basolateral extracellular domain.

(Top) Schematics of hESC epithelium on filter (Bottom) Schematics of NOGGIN transcytosis route. Note that NOGGIN (red) travels through pinocytotic vesicles, ASE, EE, CRE, and BSE. ARE is shown in blue as it is not engaged in the trafficking of NOGGIN.